Simple Formulas and Results for Buckling-Resistance and Stiffness Design of Compression-Loaded Laminated-Composite Cylinders

Michael P. Nemeth
Langley Research Center, Hampton, Virginia

Martin M. Mikulas, Jr.
National Institute of Aerospace, Hampton, Virginia

The NASA STI Program Office . . . in Profile

Since its founding, NASA has been dedicated to the advancement of aeronautics and space science. The NASA scientific and technical information (STI) program plays a key part in helping NASA maintain this important role.

The NASA STI program operates under the auspices of the Agency Chief Information Officer. It collects, organizes, provides for archiving, and disseminates NASA's STI. The NASA STI program provides access to the NASA Aeronautics and Space Database and its public interface, the NASA Technical Report Server, thus providing one of the largest collections of aeronautical and space science STI in the world. Results are published in both non-NASA channels and by NASA in the NASA STI Report Series, which includes the following report types:
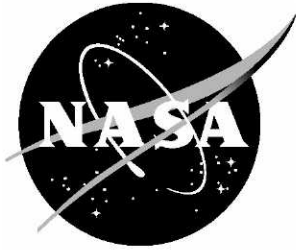
- TECHNICAL PUBLICATION. Reports of completed research or a major significant phase of research that present the results of NASA programs and include extensive data or theoretical analysis. Includes compilations of significant scientific and technical data and information deemed to be of continuing reference value. NASA counterpart of peer-reviewed formal professional papers, but having less stringent limitations on manuscript length and extent of graphic presentations.

- TECHNICAL MEMORANDUM. Scientific and technical findings that are preliminary or of specialized interest, e.g., quick release reports, working papers, and bibliographies that contain minimal annotation. Does not contain extensive analysis.

- CONTRACTOR REPORT. Scientific and technical findings by NASA-sponsored contractors and grantees.

- CONFERENCE PUBLICATION. Collected papers from scientific and technical conferences, symposia, seminars, or other meetings sponsored or co-sponsored by NASA.

- SPECIAL PUBLICATION. Scientific, technical, or historical information from NASA programs, projects, and missions, often concerned with subjects having substantial public interest.

- TECHNICAL TRANSLATION. English-language translations of foreign scientific and technical material pertinent to NASA's mission.

Specialized services also include creating custom thesauri, building customized databases, and organizing and publishing research results.

For more information about the NASA STI program, see the following:

- Access the NASA STI program home page at http://www.sti.nasa.gov

- E-mail your question via the Internet to help@sti.nasa.gov

- Fax your question to the NASA STI Help Desk at 443-757-5803

- Phone the NASA STI Help Desk at 443-757-5802

- Write to:
  NASA STI Help Desk
  NASA Center for AeroSpace Information
  7115 Standard Drive
  Hanover, MD 21076-1320

Simple Formulas and Results for Buckling-Resistance and Stiffness Design of Compression-Loaded Laminated-Composite Cylinders

Michael P. Nemeth
Langley Research Center, Hampton, Virginia

Martin M. Mikulas, Jr.
National Institute of Aerospace, Hampton, Virginia

Available from:

Summary

Simple formulas for the buckling stress of homogeneous, specially orthotropic, laminated-composite cylinders are presented that are the counterpart of the classical buckling formula for an isotropic cylinder. The formulas are obtained by using nondimensional parameters and equations that facilitate general validation, and are validated against the exact solution for a wide range of cylinder geometries and laminate constructions. The buckling stress is found to be a product of a nondimensional coefficient, that involves only material properties of the wall, with the thickness-to-radius ratio of the cylinder and the effective modulus of the corresponding quasi-isotropic laminate. Unlike the corresponding isotropic-cylinder solution, that is represented by a single equation, two equations that depend on the laminate orthotropy are needed to obtain the orthotropic-cylinder solution; one for axisymmetric and one for asymmetric buckling modes. Results are presented that establish the ranges of the nondimensional parameters and coefficients used. General results, given in terms of the nondimensional parameters, are presented that encompass a wide range of geometries and laminate constructions. These general results also illustrate a wide spectrum of behavioral trends. Design-oriented results are also presented that provide a simple, clear indication of laminate composition on critical stress, critical strain, and axial stiffness. The particular graphical form of these results that is used in the present study enables rapid trade studies for different design requirements. One conclusion found in the present study is that no buckling stress can be achieved for homogeneous specially orthotropic cylinders that is higher than the corresponding quasi-isotropic layup. Another conclusion is that the higher values of buckling stress are associated with higher values of axial strain. An example is provided to demonstrate the application of these results to thin-walled column designs.

Symbols

$A = 2\pi Rt$	cylinder cross-sectional area, in^2
$\mathcal{A}, \mathcal{B}$	nondimensional modal amplitudes defined by equations (12)-(14)
$A_{11}, A_{12}, A_{22}, A_{66}$	orthotropic-cylinder membrane stiffnesses, lb/in.
c_x	nondimensional coefficient defined by equations (43)
$\bar{c}_x$	value of c_x for quasi-isotropic laminates

1

d	bending boundary layer attenuation length defined by equation (48), in.
$D_{11}, D_{12}, D_{22}, D_{66}$	orthotropic-cylinder bending stiffnesses, in-lb
$D_m(\ ), D_c(\ ), D_b(\ )$	nondimensional linear differential operators defined by equations (3)-(5)
$\bar{E}$	effective modulus of quasi-isotropic laminates, psi
$\bar{G}$	effective shear modulus of quasi-isotropic laminates, psi
E_1, E_2, G_{12}	lamina moduli, psi
E_x, E_y, G_{xy}	effective laminate moduli, psi
$I = \pi R^3 t$	cylinder moment of inertia, in^4
$I(n_{cr})$	integer closest to the number given by equation (31)
L	cylinder length (see figure 2), in.
m	number of axial half waves in buckle pattern (see equation (12) and figure 4)
n, n_{cr}	number of circumferential waves in buckle pattern (see equation (12) and figures 3 and 4) and value at buckling, respectively
N_x, N_x^{cr}	compressive axial prebuckling stress resultant and corresponding value at buckling, respectively
$\tilde{p}, \tilde{p}_{cr}$	nondimensional loading parameter defined by equation (11) and corresponding value at buckling, respectively
$Q_{11}, Q_{12}, Q_{22}, Q_{66}$	stiffnesses of a homogeneous specially orthotropic material in a state of plane stress, psi
$\bar{Q}_{ij}^{\,0}, \bar{Q}_{ij}^{\,90}, \bar{Q}_{ij}^{\,\theta}, \bar{Q}_{ij}^{\,-\theta}$	transformed reduced stiffnesses of the 0-degree, 90-degree, and $\pm\theta$ angle plies, respectively
R	cylinder radius (see figure 2), in.
t	cylinder thickness (see figure 2), in.
t_0, t_{90}, t_θ	total thickness of the 0-degree, 90-degree, and $\pm\theta$ angle plies, respectively, in.

$\bar{t}_0 = \dfrac{t_0}{t}$, $\bar{t}_{90} = \dfrac{t_{90}}{t}$, $\bar{t}_\theta = \dfrac{t_\theta}{t}$	thickness fractions of the 0-degree, 90-degree, and $\pm\theta$ angle plies, respectively
x, y	cylinder coordinate system (see figure 2), in.
$Z = \rho\alpha_m^2$	Batdorf-Stein Z parameter
α_b, α_m	nondimensional stiffness-weighted length-to-radius ratios defined by equations (8) and (6), respectively, and by equation (17)
β	nondimensional orthotropy parameter defined by equations (9) and (19)
γ	buckling knockdown factor defined by equation (50)
δF	nondimensional buckling-stress function (see equations (1) and (2))
δW	nondimensional radial-displacement field at buckling (see equations (1) and (2))
ε	parameter defined by equation (34b)
$\dot{\varepsilon}$	bending boundary layer attenuation tolerance used in equation (48)
ε_x^{cr}, $\bar{\varepsilon}_x^{cr}$	value of the uniform axial strain at buckling and corresponding value for quasi-isotropic laminates
$\eta = \dfrac{y}{R}$	nondimensional cylinder circumferential coordinate
θ	lamina fiber angle (see figure 2), degrees
λ, λ_{cr}	stiffness-weighted axial-buckle aspect ratio defined by equation (23) and value at buckling, respectively
μ	nondimensional orthotropy parameter defined by equations (7) and (18), respectively
ν_{12}	lamina major Poisson's ratio
ν_{xy}, ν_{yx}	effective laminate major and minor Poisson's ratios, respectively
$\bar{\nu}$	effective Poisson's ratio of quasi-isotropic laminates
$\xi = \dfrac{x}{L}$	nondimensional cylinder axial coordinate

ρ

stiffness-weighted radius-to-thickness ratio defined by equations (10) and (20)

$\sigma_x^{cr} = \dfrac{N_x^{cr}}{t}, \ \bar{\sigma}_x^{cr}$

value of the uniform axial stress at buckling and corresponding value for quasi-isotropic laminates, psi

Introduction

Design of lightweight, high-performance structures is a key element of developing new spacecraft such as the Altair lunar lander shown in figure 1. For example, the present cost for placing this vehicle in Earth orbit is approximately \$10,000 per pound. As a result, fiber-reinforced, laminated-composite materials are presently being evaluated for use on Altair. These advanced composite materials have higher stiffness-to-density ratios, higher strength-to-density ratios, and very low coefficients of thermal expansion, compared to isotropic materials. In addition, because laminated composites are composed of layers of an orthotropic material, oriented at various angles, the potential exists to optimally tailor a laminate to meet a specific set of structural requirements. Thus, laminated composites offer a design space that is much wider than that for isotropic materials. However, along with the potential structural performance benefits of laminate tailoring comes a much more complicated analysis and design process.

An important component of the Altair lunar lander is the leg, which must be buckling resistant when subjected to compression loads associated with landing. One concept under consideration is a thin-walled tubular column with a circular cross section. This family of structures is commonly used in compression applications because of the enhanced load-carrying capability provided by the cross-sectional curvature. In designing the lander leg, both the local shell-wall and the overall column buckling modes must be considered. Accurate assessment of local shell-wall buckling remains a difficult problem because of the inherent sensitivity of the load-carrying capacity to initial geometric wall imperfections with amplitudes on the order of the nominal wall thickness.

Structural analysis and design methods for compression-loaded cylinders have been under development for many years. This effort has focused to a large extent on isotropic cylinders with monocoque, ring-and-stringer stiffened, or sandwich construction. For example, Switsky & Cary (reference 1) presented a nondimensional minimum-weight-design procedure in 1963 for isotropic cylinders that includes the effects of a broad range of problem variables. Similarly, Crawford and Burns (reference 2) presented structural efficiency results for isotropic cylinders with either monocoque, ring-and-stringer stiffened, or sandwich construction about the same time. Likewise, Cohen (reference 3) presented a study in 1963 on the minimum weight design of truss-core sandwich cylinders subjected to axial compression. In 1966, Dow and Rosen (reference 4) presented some simple design formulas for buckling of compression-loaded cylinders with homogeneous specially orthotropic walls and some corresponding structural efficiency results for laminated composites. Another study that focused on ring-and-stringer stiffened isotropic cylinders subjected to axial compression was presented by Burns and Almroth (reference 5) in 1966.

In 1965, the National Aeronautics and Space Administration (NASA) released a set of design recommendations for buckling of cylindrical shells, known as NASA SP 8007, which was updated in 1968 (reference 6). This reference documents analysis methods and presents empirical knockdown factors for isotropic cylinders, of various sizes and loading conditions, that account for geometric-imperfection sensitivity. These knockdown factors are based on lower bounds to empirical buckling loads determined from experiments conducted from approximately 1930 to 1967. As a result of the uncertainty in the pedigree of many of the experiments and the actual nature of the boundary conditions, these knockdown factors are expected to yield overly conservative designs. This reference also presents the classical analysis method for orthotropic cylinders that requires a search over a wide range of the possible buckling modes to determine the critical load. As a result of a general lack of experimental data, NASA SP 8007 recommends an approach for using the empirical knockdown factors obtained for isotropic cylinders to obtain a conservative estimate of the imperfection sensitivity of orthotropic cylinders. It is important to point out that no validated design data is given in NASA SP 8007 for laminated-composite cylinders.

Other studies that have addressed analysis and design methods for compression-loaded cylinders are given in references 7-19. More recently, Weaver and his colleagues (references 20-26) have presented a substantial number of results that provide insight into the analysis and design of laminated-composite cylinders subjected to compression loads. In particular, design charts that show the effects of cylinder geometry and laminate construction on the boundaries between local shell-wall buckling, overall column buckling, and compressive strength failure modes are presented in reference 20. Likewise, the effects of laminate construction on the transition from shell-wall buckling to overall column buckling and combined interactions are addressed in reference 23.

As evidenced by the references cited herein, efforts to develop shell-buckling design technology for laminated-composite cylinders have been underway for many years. Despite these efforts, the technology still has not reached the level of maturity needed to obtain the full weight-saving potential of shell structures, especially those made of laminated-composite materials. The major impediment is a lack of validated analysis and design methods. As a result, NASA SP 8007, developed in the late 1960s, is still the primary resource used by American industry for the design of buckling-resistant cylindrical shells, and is sometimes used outside of its range of validity to estimate reductions in load-carrying capability caused by initial geometric imperfections. Another impediment is the lack of relatively simple design formulas that are accurate enough to establish intuitive design trends for a broad range of problem variables. Formulas such as these provide a means for navigating a given preliminary-design space in the early phases of a building-block design process.

One objective of the present study is to present an alternate derivation of the design formulas presented by Dow and Rosen in 1966 that uses nondimensional parameters and equations to facilitate validation of the formulas for a wide range of laminate constructions. Other objectives are to illustrate the effects of laminate orthotropy on behavioral trends and the accuracy of the design formulas. Another objective is to demonstrate the use of the formulas in developing design data that captures behavioral trends for a wide range of laminate constructions, and that augments the results presented in reference 20. Specifically, plots of normalized buckling stress

versus normalized buckling strain are presented as a function of laminate composition. By including strain in these plots, both structural stiffness and load-capacity requirements can be considered in the design process. These formulas and results represent a significant first-approximation advancement in design technology for compression-loaded laminated-composite cylinders.

To accomplish these objectives, attention is limited to laminated composites whose dominant behavioral characteristics can be captured by representing the laminates as an equivalent homogeneous specially orthotropic shell wall. For example, the allowable range of structural dimensions for a design may be such that the laminate can be presumed to be composed of enough plies that are distributed uniformly through the thickness to yield, effectively, a homogeneous shell wall. As discussed by Weaver and Nemeth (reference 27), most aerospace design practices limit the use of laminated composites to those that are balanced and symmetrically laminated. Furthermore, presuming that the cylinder wall is homogeneous and specially orthotropic is not a serious limitation in a preliminary design process, in many cases. Therefore, this approach is expected to be relevant to a wide range of practical applications. In addition, this approach is a logical first step in a building-block approach to more general laminate constructions. Most importantly, this approach yields significant simplification of the buckling equations and facilitates the development of simple design formulas in terms of useful nondimensional parameters and equations.

Subsequently, a set of nondimensional linear bifurcation buckling equations and parameters are presented for balanced, symmetrically laminated cylinders subjected to uniform axial compression loads and in a membrane-stress prebuckling state. Anisotropy of the shell wall is presumed to be negligible. Then, a linear bifurcation buckling analysis is presented for the classical simply supported boundary conditions that are typically used in preliminary design of cylinders. Next, the buckling analysis is specialized to homogeneous specially orthotropic cylinders, the simplified formulas are derived, and important considerations are discussed. The equations used in the analysis to represent laminates as an equivalent homogeneous specially orthotropic shell wall are then presented, followed by results. Results that establish the range of the nondimensional parameters that appear in the buckling analysis and simplified formulas are presented first. Then, general results that establish behavioral characteristics and trends as a function of the nondimensional parameter are presented to establish the range of validity of the approximate formulas. Finally, results that show behavioral characteristics and trends as a function of laminate construction are presented that should provide an insightful design perspective for various structural requirements.

Bifurcation Equations

To accomplish the objective of the present study, it is convenient to use the nondimensional parameters and equations presented in reference 28. When specialized to right circular cylindrical shells, such as that shown in figure 2, these equations correspond to Donnell-type, linear-bifurcation buckling equations for symmetric laminates. In particular, the compatibility equation is given by

$$D_m(\delta F) = \sqrt{12}\, D_c(\delta W) \tag{1}$$

and the transverse equilibrium equation is given by

$$D_b(\delta W) + \sqrt{12}\, D_c(\delta F) = -\tilde{p}\pi^2 \frac{\partial^2 \delta W}{\partial \xi^2} \tag{2}$$

where $D_m(\ )$, $D_b(\ )$, and $D_c(\ )$ are nondimensional linear differential operators. The symbol δW denotes the nondimensional radial-displacement buckling mode and δF denotes the corresponding stress function.   For symmetric laminates with negligible coupling between inplane stretching and shearing deformations, and between pure bending and twisting deformations, these operators are given by

$$D_m(\delta F) = \frac{1}{\alpha_m^2} \frac{\partial^4 \delta F}{\partial \xi^4} + 2\mu \frac{\partial^4 \delta F}{\partial \xi^2 \partial \eta^2} + \alpha_m^2 \frac{\partial^4 \delta F}{\partial \eta^4} \tag{3}$$

$$D_c(\delta W) = \rho \frac{\partial^2 \delta W}{\partial \xi^2} \tag{4}$$

$$D_b(\delta W) = \frac{1}{\alpha_b^2} \frac{\partial^4 \delta W}{\partial \xi^4} + 2\beta \frac{\partial^4 \delta W}{\partial \xi^2 \partial \eta^2} + \alpha_b^2 \frac{\partial^4 \delta W}{\partial \eta^4} \tag{5}$$

The nondimensional coordinates in these equations are defined as $\xi = \frac{x}{L}$ and $\eta = \frac{y}{R}$, where x is the axial coordinate, y is the circumferential arc-length coordinate, L is the cylinder length, R is the cylinder radius, $0 \le \xi \le 1$, and $0 \le \eta \le 2\pi$. The nondimensional parameters appearing in these equations are given by

$$\alpha_m = \frac{L}{R}\left(\frac{A_{22}}{A_{11}}\right)^{\frac{1}{4}} \tag{6}$$

$$\mu = \frac{A_{11}A_{22} - A_{12}^2 - 2A_{12}A_{66}}{2A_{66}\sqrt{A_{11}A_{22}}} \tag{7}$$

$$\alpha_b = \frac{L}{R}\left(\frac{D_{22}}{D_{11}}\right)^{\frac{1}{4}} \tag{8}$$

$$\beta = \frac{D_{12} + 2D_{66}}{\sqrt{D_{11}D_{22}}} \tag{9}$$

$$\rho = \frac{R}{t} \sqrt{\frac{\left(A_{11}A_{22} - A_{12}^2\right)t^2}{12\sqrt{A_{11}A_{22}D_{11}D_{22}}}} \tag{10}$$

where A_{11}, A_{12}, A_{22}, A_{66}, D_{11}, D_{12}, D_{22}, and D_{66} are the stiffnesses of classical laminated-shell theory, and the corresponding stiffnesses A_{16}, A_{26}, D_{16}, and D_{26} are presumed negligible. The parameter defined by equation (10) is a stiffness-weighted thinness parameter, not the Batdorf-Stein Z parameter defined in reference 27. An analogue of the Batdorf-Stein Z parameter, that reduces to the Batdorf Z parameter for isotropic shells, is given by the quantity $Z = \rho\alpha_m^2$. The quantity $\tilde{p}$ is the loading parameter defined by

$$\tilde{p} = \frac{N_x R^2}{\pi^2 \sqrt{D_{11}D_{22}}} \tag{11}$$

where N_x is the magnitude of the uniform compressive axial stress resultant that is presumed to exist prior to buckling, in classical linear bifurcation analyses.

Buckling Analysis

For the purpose of preliminary design, cylinders with simply supported edges that restrict circumferential displacements are often used and presumed to yield conservative designs. These boundary conditions are usually referred to as the classical boundary conditions for simply supported shells. The nondimensional buckling mode for these boundary conditions is given by

$$\delta W = \mathscr{A} \sin(m\pi\xi)\cos(n\eta) \tag{12}$$

where $0 \le \xi \le 1$, $0 \le \eta \le 2\pi$, $m = 1, 2, 3, \ldots$ is the number of axial half-waves, $n = 0, 1, 2, \ldots$ is the number of full circumferential waves (see figure 3), and $\mathscr{A}$ is the indeterminate modal amplitude. A typical buckling mode is shown in figure 4a that exhibits one full axial wave and four full circumferential waves. The corresponding contour plot of the radial displacement is shown in figure 4b. Buckling modes with $n = 0$ and $n \ne 0$ are referred to herein as axisymmetric and asymmetric modes, respectively.

Substituting equation (12) into equation (1) indicates that the stress function can be represented by

$$\delta F = \mathscr{B} \sin(m\pi\xi)\cos(n\eta) \tag{13}$$

where $\mathscr{B}$ is related to the amplitude $\mathscr{A}$. Specifically, substituting equations (12) and (13) into equation (1) yields

$$\mathcal{B} = -\left[\frac{2\sqrt{3}\,\rho\,m^2\pi^2}{n^4\alpha_m^2 + 2\mu n^2 m^2\pi^2 + \dfrac{m^4\pi^4}{\alpha_m^2}} \right]\mathcal{A} \tag{14}$$

Substituting equation (14) into equation (13) and the result into equation (2), along with equation (12), and setting the coefficient of the trigonometric functions equal to zero yields the following equation for the eigenvalues $\tilde{p} = \tilde{p}(m, n)$

$$\tilde{p}\pi^2 = \frac{n^4\alpha_b^2}{m^2\pi^2} + 2\beta n^2 + \frac{m^2\pi^2}{\alpha_b^2} + \frac{12\rho^2}{\dfrac{n^4\alpha_m^2}{m^2\pi^2} + 2\mu n^2 + \dfrac{m^2\pi^2}{\alpha_m^2}} \tag{15}$$

For a given set of material properties and cylinder dimensions, the nondimensional parameters appearing in equation (15) are fixed values. The nondimensional buckling load, $\tilde{p}_{cr}$, is then given by the smallest value of $\tilde{p}$ that is found for $m = 1, 2, 3, \ldots$ and $n = 0, 1, 2, \ldots$. The corresponding wave numbers are denoted by m_{cr} and n_{cr}.

Equations for Homogeneous Orthotropic Cylinders

For an orthotropic cylinder with a homogeneous wall construction, the shell stiffnesses are given by

$$\begin{bmatrix} A_{11} & A_{12} & 0 \\ A_{12} & A_{22} & 0 \\ 0 & 0 & A_{66} \end{bmatrix} = t \begin{bmatrix} Q_{11} & Q_{12} & 0 \\ Q_{12} & Q_{22} & 0 \\ 0 & 0 & Q_{66} \end{bmatrix} \tag{16a}$$

and

$$\begin{bmatrix} D_{11} & D_{12} & 0 \\ D_{12} & D_{22} & 0 \\ 0 & 0 & D_{66} \end{bmatrix} = \frac{t^3}{12} \begin{bmatrix} Q_{11} & Q_{12} & 0 \\ Q_{12} & Q_{22} & 0 \\ 0 & 0 & Q_{66} \end{bmatrix} \tag{16b}$$

where expressions for Q_{11}, Q_{12}, Q_{22}, and Q_{66} are the stiffnesses of a single layer of homogeneous orthotropic material in a state of plane stress, referred to the principal material coordinate system. Expressions for these stiffnesses are found, in terms of material properties, in reference 29 (see pp. 70-73). Herein, the major and minor principal material coordinate frames are taken to be aligned with the x and y coordinate frame shown in figure 2. For this special case, the nondimensional parameters given by equations (6) - (10) become

$$\alpha_m = \alpha_b = \frac{L}{R}\left(\frac{Q_{22}}{Q_{11}}\right)^{\frac{1}{4}} \tag{17}$$

$$\mu = \frac{Q_{11}Q_{22} - Q_{12}^2 - 2Q_{12}Q_{66}}{2Q_{66}\sqrt{Q_{11}Q_{22}}} \tag{18}$$

$$\beta = \frac{Q_{12} + 2Q_{66}}{\sqrt{Q_{11}Q_{22}}} \tag{19}$$

$$\rho = \frac{R}{t}\sqrt{1 - \frac{Q_{12}^2}{Q_{11}Q_{22}}} \tag{20}$$

The bifurcation buckling loads defined by equations (11) and (15) become

$$\tilde{p}\pi^2 = \frac{12N_xR^2}{\sqrt{Q_{11}Q_{22}}\,t^3} = \frac{n^4\alpha_m^2}{m^2\pi^2} + 2\beta n^2 + \frac{m^2\pi^2}{\alpha_m^2} + \frac{12\rho^2}{\dfrac{n^4\alpha_m^2}{m^2\pi^2} + 2\mu n^2 + \dfrac{m^2\pi^2}{\alpha_m^2}} \tag{21}$$

To obtain a simple, approximate design formula, similar to that given in reference 4, equation (21) is differentiated as if $\tilde{p} = \tilde{p}(m, n)$ is a continuous function and m and n are real variables. Although not strictly correct, this approach gives useful results for certain ranges of the nondimensional parameters appearing in equation (21). To obtain a minimum set,

$$d\tilde{p} = \frac{\partial\tilde{p}}{\partial m}\,dm + \frac{\partial\tilde{p}}{\partial n}\,dn = 0 \tag{22}$$

To clarify matters, note that

$$\frac{\alpha_m}{m\pi} = \frac{L}{\pi mR}\left(\frac{Q_{22}}{Q_{11}}\right)^{\frac{1}{4}} \equiv \lambda \tag{23}$$

Because m is the number of axial half waves in a given bifurcation eigenvector, the quantity L/m is the axial half-wave length of the eigenvector, and λ represents a stiffness-weighted axial-buckle aspect ratio. As the cylinder length increases, λ behaves like a continuous variable and minimization of equation (21) by differentiation with respect to λ represents solutions for an infinitely long cylinder that buckles into a local shell mode and not into an overall column mode. By using equation (23), equation (21) becomes

$$\tilde{p}\pi^2 = n^4\lambda^2 + 2\beta n^2 + \frac{1}{\lambda^2} + \frac{12\rho^2}{n^4\lambda^2 + 2\mu n^2 + \dfrac{1}{\lambda^2}} \tag{24}$$

Enforcing $\dfrac{\partial\tilde{p}}{\partial\lambda} = 0$ gives

$$\left(n^4 - \frac{1}{\lambda^4}\right)\left\{\left[n^4 + \frac{2\mu n^2}{\lambda^2} + \frac{1}{\lambda^4}\right]^2 - \frac{12\rho^2}{\lambda^4}\right\} = 0 \tag{25}$$

Likewise, enforcing $\dfrac{\partial \tilde{p}}{\partial n} = 0$ gives

$$\left(n^2 + \frac{\beta}{\lambda^2}\right)\left[n^4 + \frac{2\mu n^2}{\lambda^2} + \frac{1}{\lambda^4}\right]^2 - \frac{12\rho^2}{\lambda^4}\left(n^2 + \frac{\mu}{\lambda^2}\right) = 0 \tag{26}$$

Inspection of equations (25) and (26) indicates that when $\beta = \mu$, both equations are satisfied when

$$n^4 + \frac{2\mu n^2}{\lambda^2} + \frac{1}{\lambda^4} = -\frac{\sqrt{12}\rho}{\lambda^2} \tag{27a}$$

and

$$n^4 + \frac{2\mu n^2}{\lambda^2} + \frac{1}{\lambda^4} = \frac{\sqrt{12}\rho}{\lambda^2} \tag{27b}$$

Substituting equation (27a) into equation (24) gives

$$\tilde{p}_{cr} = -\frac{4\sqrt{3}\,\rho}{\pi^2} \tag{28a}$$

which is physically inadmissible. Similarly, equation (27b) gives

$$\tilde{p}_{cr} = \frac{4\sqrt{3}\,\rho}{\pi^2} \tag{28b}$$

Thus, equation (27b), with $n = n_{cr}$ and $\lambda = \lambda_{cr}$, and equation (28b) correspond to the physical solution for $n = 0, 1, 2, \dots$.

For the general case of $\beta \neq \mu$, a solution to equations (25) and (26) is found for values of $n \neq 0$ as follows. Equation (25) is satisfied by picking $n = \frac{1}{\lambda}$ and then substituting this value into equation (26) to get

$$(1 + \beta)(1 + \mu) - 3\rho^2\lambda^4 = 0 \tag{29}$$

which yields

$$\lambda_{cr} = \left[\frac{(1 + \beta)(1 + \mu)}{3\rho^2} \right]^{\frac{1}{4}} \tag{30}$$

Substituting this result into $n = \frac{1}{\lambda}$ gives

$$n_{cr} = \left[\frac{3\rho^2}{(1 + \beta)(1 + \mu)} \right]^{\frac{1}{4}} \tag{31}$$

Next, equations (30) and (31) are substituted into equation (24) to get

$$\tilde{p}_{cr} = \frac{12 N_x^{cr} R^2}{\pi^2 \sqrt{Q_{11} Q_{22}} \, t^3} = \frac{4\sqrt{3}\,\rho}{\pi^2} \sqrt{\frac{1 + \beta}{1 + \mu}} \tag{32a}$$

for values of $n = 1, 2, \dots$. Observe that this equation includes the solution for the case of $\beta = \mu$ given by equation (28b). The solution for the case of $n = 0$ is obtained by substituting $n = 0$ into equation (24) and then minimizing with respect to λ. The results are

$$\tilde{p}_{cr} = \frac{4\sqrt{3}\,\rho}{\pi^2} \tag{32b}$$

$$\lambda_{cr} = \left[12\rho^2 \right]^{-\frac{1}{4}} \tag{32c}$$

Thus, for a given set of problem parameters, the critical load is given by the smallest value of equations (32a) and (32b). Inspection of these equations reveals that the $n = 0$ solution given by equation (32b) is the smallest for values of $\beta > \mu$.

In general, equation (31), for $n \neq 0$, yields non-integer values for n_{cr} because n has been treated as a continuous variable in the minimization process. Thus, the periodicity of the buckle pattern defined by equation (12), and illustrated in figure 3, is generally violated, which introduces errors into the solution. To obtain the correct solution for an infinitely long cylinder, n_{cr} must be an integer. An improved solution is obtained by defining

$$n_{cr}^{\infty} = n_{cr}(1 + \varepsilon) \tag{33a}$$

and

$$\lambda_{cr}^{\infty} = \frac{1}{n_{cr}^{\infty}} \tag{33b}$$

Substituting equation (33a) for n and (33b) for λ into equation (24) gives

$$\tilde{p}_{cr} = \frac{12N_x^{cr}R^2}{\pi^2\sqrt{Q_{11}Q_{22}}\,t^3} = \frac{2\sqrt{3}\,\rho}{\pi^2}\sqrt{\frac{1+\beta}{1+\mu}}\left(1 + 2\varepsilon + \varepsilon^2 + \frac{1}{1+2\varepsilon+\varepsilon^2}\right) \tag{34a}$$

The improvement in the solution now comes down to the choice of ε. In the present study,

$$\varepsilon = \frac{I(n_{cr}) - n_{cr}}{n_{cr}} \tag{34b}$$

is used, where $I(n_{cr})$ denotes the integer closest to the number given by equation (31).

An expression for the critical stress of a geometrically perfect cylinder, for the general case of $\beta \neq \mu$ and the special case of $\beta = \mu$, is obtained directly from the equation (34a). Using equation (20) and the formula for the critical stress, $\sigma_x^{cr} = \dfrac{N_x^{cr}}{t}$, equation (34a) becomes

$$\sigma_x^{cr} = \frac{t}{2\sqrt{3}R}\sqrt{Q_{11}Q_{22} - Q_{12}^2}\sqrt{\frac{1+\beta}{1+\mu}}\left(1 + 2\varepsilon + \varepsilon^2 + \frac{1}{1+2\varepsilon+\varepsilon^2}\right) \tag{35}$$

In terms of the properties of a homogeneous orthotropic material,

$$\sqrt{Q_{11}Q_{22} - Q_{12}^2} = \sqrt{\frac{E_xE_y}{1 - \nu_{xy}\nu_{yx}}} \tag{36}$$

$$\beta = \sqrt{\nu_{xy}\nu_{yx}} + \frac{2G_{xy}}{\sqrt{E_xE_y}}\left(1 - \nu_{xy}\nu_{yx}\right) \tag{37}$$

$$\mu = \frac{\sqrt{E_xE_y}}{2G_{xy}} - \sqrt{\nu_{xy}\nu_{yx}} \tag{38}$$

$$\rho = \frac{R}{t}\sqrt{1 - \nu_{xy}\nu_{yx}} \tag{39}$$

and

$$\alpha_m = \frac{L}{R}\left(\frac{E_y}{E_x}\right)^{\frac{1}{4}} \tag{40}$$

In these equations, the subscripts x and y have been used to designate the major and minor principal material coordinates, instead of the subscripts 1 and 2, respectively, found in reference 29. After simplification, equation (35) becomes

$$\sigma_x^{cr} = \frac{1}{2}\sqrt{\frac{2G_{xy}\sqrt{E_xE_y}}{3\left(1 - \sqrt{\nu_{xy}\nu_{yx}}\right)}}\left(1 + 2\varepsilon + \varepsilon^2 + \frac{1}{1+2\varepsilon+\varepsilon^2}\right)\frac{t}{R} \tag{41a}$$

and equation (32b) for $n = 0$ becomes

$$\sigma_x^{cr} = \sqrt{\frac{E_x E_y}{3(1 - \nu_{xy}\nu_{yx})}} \; \frac{t}{R} \tag{41b}$$

When the effect of ε on σ_x^{cr} is negligible, the critical stress of equation (41a) is given by

$$\sigma_x^{cr} = \sqrt{\frac{2G_{xy}\sqrt{E_x E_y}}{3(1 - \sqrt{\nu_{xy}\nu_{yx}})}} \; \frac{t}{R} \tag{42a}$$

which is the same as that given by Dow and Rosen (reference 4). Also, equations (41b) and (42a) reduce to the well-known formula

$$\sigma_x^{cr} = \frac{E}{\sqrt{3(1 - \nu^2)}} \left(\frac{t}{R}\right) \tag{42b}$$

for isotropic cylinders (see reference 30). In contrast to reference 20, equations (41b) and (42a) are expressed in the form

$$\sigma_x^{cr} = c_x \overline{E} \left(\frac{t}{R}\right) \tag{43a}$$

where c_x is the smallest value of

$$c_x = \sqrt{\frac{2\dfrac{G_{xy}}{\overline{E}}\left(\dfrac{E_x}{\overline{E}}\right)^{\frac{1}{2}}\left(\dfrac{E_y}{\overline{E}}\right)^{\frac{1}{2}}}{3(1 - \sqrt{\nu_{xy}\nu_{yx}})}} \quad \text{for } n \neq 0 \tag{43b}$$

$$c_x = \sqrt{\frac{\left(\dfrac{E_x}{\overline{E}}\right)\left(\dfrac{E_y}{\overline{E}}\right)}{3(1 - \nu_{xy}\nu_{yx})}} \quad \text{for } n = 0 \tag{43c}$$

In equations (43), $\overline{E}$ is the effective elastic modulus of the corresponding quasi-isotropic laminate. The critical strain is given by

$$\varepsilon_x^{cr} = \frac{\sigma_x^{cr}}{E_x} = c_x \frac{\overline{E}}{E_x}\left(\frac{t}{R}\right) \tag{44}$$

It is also convenient to define, with regard to presentation of results, the critical stress and strain for the corresponding quasi-isotropic laminate as

$$\bar{\sigma}_x^{cr} = \bar{c}_x \bar{E} \left(\frac{t}{R} \right) \tag{45a}$$

$$\bar{\varepsilon}_x^{cr} = \bar{c}_x \left(\frac{t}{R} \right) \tag{45b}$$

where $\bar{c}_x$ is given by

$$\bar{c}_x = \sqrt{\frac{2\frac{\bar{G}}{\bar{E}}}{3\left(1 - \bar{\nu}\right)}} = \frac{1}{\sqrt{3\left(1 - \bar{\nu}^2\right)}} \tag{45c}$$

for all values of n, and $\bar{G}$ and $\bar{\nu}$ are the effective shear modulus and Poisson's ratio. With these representations, it follows that

$$\frac{\sigma_x^{cr}}{\bar{\sigma}_x^{cr}} \left(\frac{\bar{\varepsilon}_x^{cr}}{\varepsilon_x^{cr}} \right)^{-1} = \frac{E_x}{\bar{E}} \tag{46}$$

Important Considerations

It is important to note that Donnell's equations are typically inaccurate for small, nonzero values of the circumferential wave number n. Let $\tilde{n}$ denote the lower bound of n_{cr} for which Donnell's equations are presumed to be accurate; i. e., $n_{cr} \geq \tilde{n}$. Equation (31) yields

$$\rho \geq \tilde{n}^2 \sqrt{\frac{\left(1 + \beta\right)\left(1 + \mu\right)}{3}} \tag{47}$$

This equation gives an estimate of the range of ρ that Donnell's equations are expected to be accurate. The ranges of β and μ are defined by the shell wall construction (e. g., see reference 27).

In the formulation of the Donnell-type linear bifurcation equations presented herein, the compression-loaded cylinder is presumed to be in a membrane compression-stress state prior to buckling. This presumption implies that the zones of bending stresses induced by radial restraint at the boundaries are small compared to the length of the cylinder, and that the bending stresses have a second-order influence on the onset of buckling. As a result, it is important to have an expression for the attenuation length of the bending-stress zones, denoted herein as d. The desired expression is presented in reference 31 (see (19) and (21)) and given here as

$$d = -\ln\bar{\varepsilon} \sqrt{Rt} \left[\frac{E_x}{3E_y\left(1 - \nu_{xy}\nu_{yx}\right)} \right]^{\frac{1}{4}} \tag{48}$$

where $\bar{\varepsilon}$ denotes a prescribed attenuation tolerance. For 90% response attenuation, $\bar{\varepsilon} = 0.1$ and $-\ln\bar{\varepsilon} = 2.30$.

Another important consideration is the stress level at which a long simply supported cylinder buckles into an overall column mode. This stress level was derived from the equations given in reference 32 (see pp. 171-173) and is given by

$$\sigma_x^{cr} = \sigma_x^{Euler}\left[1 + \frac{2}{3}\left(\frac{\pi R}{L}\right)^2 \frac{E_x}{G_{xy}}\right]^{-1} \tag{49a}$$

This expression includes the effects of transverse shear flexibility of a thin-walled circular cylinder. The Euler stress, which neglects transverse shear flexibility, is given by

$$\sigma_x^{Euler} \equiv \frac{\pi^2 E_x I}{AL^2} = \frac{\pi^2}{2}\left(\frac{R}{L}\right)^2 E_x \tag{49b}$$

where the moment of inertia for a thin-walled circular cylinder, $I = \pi R^3 t$, has been used and $A = 2\pi R t$ is the cross-sectional area.

It is also important to note that equation (43a) does not account for the reduction in load-carrying capacity associated with the presence of initial geometric imperfections. Therefore, the critical stress should be multiplied by a knockdown factor γ such as

$$\gamma = 1 - 0.901\left(1 - e^{-\frac{1}{16}\sqrt{\frac{R}{t}}}\right) \tag{50}$$

This knockdown factor is that given in NASA SP 8007 for orthotropic cylinders, but modified for the case of a homogeneous specially orthotropic material by using equations (16). It is worth noting that equation (50) is identical to the knockdown-factor equation in NASA SP 8007 for isotropic cylinders, and is a lower bound to experimental data that is expected to yield very conservative, and possibly overweight, designs.

Representation of Laminates as Homogeneous Orthotropic Materials

The practical wall constructions considered in the present study are laminated composites that consist of three families of plies. These three families are 0-degree, 90-degree, and $\pm\theta$ angle plies. The positive value of the fiber angle associated with a specific ply, θ, is shown in figure 2. The total thickness of the 0-degree, 90-degree, and $\pm\theta$ angle plies are denoted by t_0, t_{90}, and t_θ, respectively, and the corresponding thickness fractions are $\bar{t}_0 = \frac{t_0}{t}$, $\bar{t}_{90} = \frac{t_{90}}{t}$, and $\bar{t}_\theta = \frac{t_\theta}{t}$, where t is the total laminate thickness. Following standard practice, the membrane stiffnesses of the

laminated-composite wall, A_{ij} (see equation (16a)), are given in terms of the x-y cylinder coordinate system by

$$A_{ij} = \overline{Q}_{ij}^{0} t_0 + \overline{Q}_{ij}^{90} t_{90} + \frac{1}{2}\left(\overline{Q}_{ij}^{\theta} + \overline{Q}_{ij}^{-\theta}\right) t_{\theta} \qquad (51)$$

where $\overline{Q}_{ij}^{0}$, $\overline{Q}_{ij}^{90}$, $\overline{Q}_{ij}^{\theta}$, and $\overline{Q}_{ij}^{-\theta}$ are the transformed reduced stiffnesses of the 0-degree, 90-degree, and $\pm\theta$ angle plies, respectively, commonly used in classical laminated-plate theory (see reference 29). Applying equation (16a), the corresponding stiffnesses of a single layer of homogeneous orthotropic material are given by

$$Q_{ij} = \overline{Q}_{ij}^{0} \hat{t}_0 + \overline{Q}_{ij}^{90} \hat{t}_{90} + \frac{1}{2}\left(\overline{Q}_{ij}^{\theta} + \overline{Q}_{ij}^{-\theta}\right) \hat{t}_{\theta} \qquad (52)$$

With the homogenized stiffnesses Q_{ij} known, the corresponding engineering constants are given by

$$E_x = Q_{11} - \frac{Q_{12}^{2}}{Q_{22}} \qquad (53a)$$

$$E_y = Q_{22} - \frac{Q_{12}^{2}}{Q_{11}} \qquad (53b)$$

$$\nu_{xy} = \frac{Q_{12}}{Q_{22}} \qquad (53c)$$

$$\nu_{yx} = \frac{Q_{12}}{Q_{11}} \qquad (53d)$$

$$G_{xy} = Q_{66} \qquad (53e)$$

Results and Discussion

In the present section, results that establish the ranges of the nondimensional parameters and coefficients defined by equations (17)-(20) are presented first. Then, general results that are given in terms of the nondimensional parameters are presented that encompass a wide range of geometries and laminate constructions. These general results also illustrate a wide spectrum of behavioral trends. Finally, design-oriented results are presented that provide a simple, clear indication of the effects of laminate composition on critical stress, critical strain, and axial stiffness. In many of the figures presented herein, colored curves are used to enhance clarity of the results.

Parameter and Coefficient Ranges

To establish the range of validity of equations (32b) and (34a), the values of the nondimensional parameters defined by equations (17) - (20) were computed for several laminate configurations. In these calculations, the material properties for a generic graphite-epoxy material were used. These properties are the elastic moduli $E_1 = 20.0$ Msi and $E_2 = 2.3$ Msi, the shear modulus $G_{12} = 0.6$ Msi, and major Poisson's ratio $v_{12} = 0.3$.

Values of the parameters β and μ are shown in figures 5 and 6, respectively, for shell walls with a baseline content of 10% 90-degree plies, as a function of the fiber angle θ. Eight curves are shown in each figure that correpond to shell walls comprised of percentages of 0-degree plies that range from 10% to 80%. Similar results are shown in figures 7 and 8 for shell walls with a baseline content of 50% 90-degree plies. Five curves are shown in figures 7 and 8 for percentages of 0-degree plies that range from 0% to 40%. The results in these four figures, along with results for other intermediate cases, indicate that $0.17 \leq \beta \leq 1.75$ and $-0.03 \leq \mu \leq 9.29$. The larger values of β occur for values of θ near 45 degrees and shell walls with 10% 0-degree plies. In contrast, the smaller values of μ occur for values of θ near 45 degrees and shell walls with 10% 0-degree plies.

To simplify the validation process, the parameters β and μ were computed as parametric functions of the fiber angle θ for various percentages of 0-degree and 90-degree plies. These results form the curve shown in figure 9. By using a least-square fit, the parameter μ is expressed in terms of β by

$$\mu = -1.26 + 3.17e^{-\beta} + 87.16e^{-2\beta} - 717.12e^{-3\beta} + 2875.2e^{-4\beta} - 6559.92e^{-5\beta} + 8736.38e^{-6\beta} - 6328.33e^{-7\beta} + 1942.14e^{-8\beta} \tag{54}$$

With this equation, the parameter μ becomes a passive parameter in the validation process.

Values of the coefficients that multiply α_m in equation (40) and ρ in equation (39) are shown in figures 10 and 11, respectively, for a baseline content of 10% 90-degree plies, as a function of the fiber angle θ. In addition, the coefficient of the analogue of the Batdorf Z parameter given by

$$Z = \rho\alpha_m^2 = \frac{L^2}{Rt} \sqrt{\left(1 - \frac{Q_{12}^2}{Q_{11}Q_{22}}\right)\frac{Q_{22}}{Q_{11}}} = \frac{L^2}{Rt} \sqrt{\left(1 - v_{xy}v_{yx}\right)\frac{E_y}{E_x}} \tag{55}$$

is shown in figure 12. Eight curves are shown in each figure that correpond to shell walls comprised of percentages of 0-degree plies that range from 10% to 80%. Similar curves are presented in figures 13-15 for a baseline content of 50% 90-degree plies, as a function of the fiber angle θ. Five curves are shown in each of these figures that correpond to shell walls comprised of percentages of 0-degree plies that range from 0% to 40%.

The results in figures 10 and 13 show an increase in the moduli ratio $(E_y/E_x)^{1/4}$ as the fiber angle increases and as the percentage of 0-degree plies decreases. Moreover, the results show

that $0.69 \le (E_y/E_x)^{1/4} \le 1.72$ and that the moduli ratio generally increases as the percentage of 90-degree plies increases. In contrast, the results in figures 11 and 14 show reductions in $\sqrt{1 - \nu_{xy}\nu_{yx}}$ as the fiber angle increases to 45 degrees, followed by increases as θ increases further. The largest and smallest reductions are exhibited by the laminates with 10% and 80% zero-degree plies, respectively. The results also indicate that $0.81 \le \sqrt{1 - \nu_{xy}\nu_{yx}} \le 1.00$, and that $\sqrt{1 - \nu_{xy}\nu_{yx}}$ generally diminishes as the percentage of 90-degree plies increases. The results in figures 12 and 15 exhibit trends similar to those in figures 10 and 13, and $0.47 \le \sqrt{\left(1 - \nu_{xy}\nu_{yx}\right)\dfrac{E_y}{E_x}} \le 2.94$.

General Results

The nondimensional buckling loads given by equations (32b) and (34a) are shown in figures 16-22 as a function of the stiffness-weighted length-to-radius ratio α_m defined by equation (17). Eight curves that correspond to values of the orthotropy parameter $0.2 \le \beta \le 1.6$ are shown in figures 16-18 for values of the stiffness-weighted thinness ratio $\rho = 25$, 100, and 200, respectively. Similarly, seven curves for selected values of $25 \le \rho \le 250$ are shown in figures 19-22 for values of $\beta = 0.2$, 0.6, 1, and 1.6, respectively. The results in all these figures show a series of festoon curves in which the amplitudes of the festoons attenuate to a negligible magnitude as the stiffness-weighted length-to-radius ratio α_m increases. Likewise, the nondimensional buckling loads for a given curve attenuate to the constant value associated with an infinitely long cylinder that buckles into a local shell mode, not an overall column mode. Moreover, this value of the nondimensional buckling load provides a very useful, practical lower bound to the corresponding festoon curve. Generally, the results in figures 16-22 also show that as β, or ρ, increases the number of festoons making up a curve increases, and the concentration of festoons shifts toward $\alpha_m = 0$.

The practical lower bound character of the nondimensional buckling load of an infinitely long cylinder that buckles into a local shell mode and not an overall column mode is shown quantitatively in figure 23 for $\beta = 0.2$ and $\rho = 25$. The black festoon curve was obtained by minimizing equation (21) with respect to the buckling-mode wave numbers m and n. The horizontal blue and red lines were obtained by using equations (34) and (32), respectively, as indicated by the superscripts on the nondimensional buckling loads shown. The relatively small improvement in the lower bound predicted by these equations is associated with enforcing circumferential periodicity by using equations (33) and (34). The corresponding percent differences are shown in figure 24 and indicate that an improvement of about 1.5% is obtained by enforcing circumferential periodicity for this case.

To assess the relative accuracy of equations (32) and (34), for the range of parameters previously described herein, the nondimensional buckling loads for an infinitely long cylinder obtained from equations (24), (32), and (34) were computed for $0.2 \le \beta \le 1.8$, in increments of 0.01, and for $\rho = 25$, 50, 75, 100, 150, 200, 250, and 500. Some selections of these results are presented in Tables 1-5. The solutions obtained from minimization of equation (24) with respect

to the axial half-wave length λ and the circumferential wave number n are the most accurate of the three solutions. For every combination, the magnitude of the overall maximum difference between equations (24) and (32) was found to be less than 2.5%, with the difference decreasing substantially as ρ increases. For $\rho \geq 75$, the maximum difference is less than 1.1%. Likewise, the magnitude of the overall maximum difference between equations (24) and (34), for which circumferential periodicity is enforced, was found to be less that 0.9%, and in most cases, the magnitude of the maximum difference was significantly smaller.

Design-Oriented Results

 The results presented in figures 16-22 for finite-length cylinders suggest that equations (43) and (44) are well-suited for designing cylinders of moderate length. In addition, because of the uncertainty usually involved with material properties and other items, these equations should yield practical, conservative estimates of the response for values of the stiffness-weighted length-to-radius ratio where the festoons are prominent. That is, designing a cylinder to take advantage of load-carrying capacity in the peak of a festoon curve is likely to have significant risk associated with it if the festoons are steep and densely packed.

 Critical stress as a function of critical strain. In many design applications, the axial stiffness of a cylinder is as important as its buckling load. To provide insight into these designs, critical stresses and strains for homogeneous orthotropic cylinders, obtained from equations (43)-(46), are plotted in the generic form illustrated in figure 25. The curve shown in this figure gives a critical stress ratio as a parametric function of a critical strain ratio, in which the percentage of 0-degree plies is a continuously varying parameter and the fiber angle and percentage of 90-degree plies are fixed values. Values of the parameter increase monotonically from a value of zero, which is indicated on the curve by the filled black circular symbol (origin). The unfilled circular symbols represent values of the parameter that correspond to 10% increments, and the filled square symbol denotes 50% 0-degree plies. Altogether, the symbols are used to define an arc-length coordinate system for the curve. The critical stresses and strains in this figure are normalized by the critical stress $\bar{\sigma}_x^{cr}$ and strain $\bar{\varepsilon}_x^{cr}$ of the corresponding quasi-isotropic laminate, respectively (see equations (45)). Thus, laminate constructions with the coordinates $(1, 1)$ on the graph correspond to a quasi-isotropic laminate. In addition, the normalized-stiffness line passing through an arbitrary point of the curve has the slope given by equation (46). For the graphite-epoxy material used in the present study, the effective modulus and Poisson's ratio used in equations (45) are given by $\bar{E} = 7.89$ Msi and $\bar{v} = 0.34$, respectively. For these values, equation (45c) yields $\bar{c}_x = 0.61$.

 The utility of the graph shown in figure 25 becomes apparent by noting that as the curve is traversed by increasing the percentage of 0-degree plies, the axial stiffness increases, with a maximum value exhibited for 100% 0-degree plies, as expected. In addition, the critical strain decreases and the critical stress increases, up to a maximum value and then diminishes monotonically to a minimum value. This transition point is associated with the transition from solutions associated with $n = 0$ to those with $n \neq 0$ (see equations (43)). The $n = 0$ solutions in

figure 25 correspond to points on the curve with $\dfrac{\varepsilon_x^{cr}}{\bar{\varepsilon}_x^{cr}} \geq 1$. Although the maximum point shown on the curve in this figure is at the point (1, 1) and corresponds to a quasi-isotropic laminate, it generally does not.

Curves similar to the one shown in figure 25 are shown in figures 26-28 for values of the fiber angle $\theta = 30$, 45, and 60, respectively. Five curves are shown in each figure that correspond to distinct values of 0%, 10%, 25%, 33.33%, and 50% 90-degree plies. For each curve, the percentage of 0-degree plies (the arc-length parameter) ranges for 0% to 100% minus the percentage of 90-degree plies. One curve in each of these figures passes through the point (1, 1) and the corresponding quasi-isotropic stacking sequence is indicated on each figure. Curves similar to the one shown in figure 25 are also shown in figures 29-33 for values of the percentage of 90-degree plies = 0%, 10%, 25%, 33.33%, and 50%, respectively. Three curves are shown in each figure that correspond to distinct values of the fiber angle $\theta = 30$, 45, and 60, respectively. For each of these curves, the percentage of 0-degree plies (the arc-length parameter) also ranges from 0% to 100% minus the percentage of 90-degree plies. The results in figures 26-33 give a simple, clear indication of how fiber angle, percentage of 0-degree plies, and percentage of 90-degree plies can be adjusted to meet stress, strain, and stiffness requirements.

Column design considering local buckling. The design of an efficient thin-walled column requires a high local wall-buckling resistance and a high axial stiffness, needed to resist overall column buckling. The trade off between these two design quantities is clearly illustrated in figures 25-33, as a function of laminate construction. Although a quasi-isotropic laminate always provides the highest possible wall-buckling stress, for a given radius and thickness, the effective axial stiffness of the laminate is only about 40% of the lamina modulus, E_1. To demonstrate the potential for designing laminates with higher axial stiffness, consider the critical-stress-versus-critical-strain results presented in figure 29 for laminates with no 90-degree plies and the optimized column design presented in reference 23. This optimized design corresponds to the 16-ply laminate, $(\pm 55/0_6)_s$, which has 75% 0-degree plies that are "sandwiched" between relatively thin angle-ply face-sheet layers. The buckling load for this laminate was obtained by using equation (15), which presumes that the effects of anisotropy in the form of coupling between bending and twisting are negligible. The results in figure 29 are reproduced in figure 34, along with results for the optimized design of reference 23. However, in figure 34, the arc-length coordinates have been omitted for clarity. In assessing the merit of a design, it is important to note that the left-hand-most portion of the curves represents the maximum values of stiffness (lower strain) for a given buckling-stress level of a homogeneous orthotropic cylinder.

The filled circular symbol shown on figure 34 corresponds to the optimized design presented in reference 23. Since this data point is slightly to the left of the curves for the homogeneous orthotropic laminates, the design is more structurally efficient. The data point that corresponds to representing the $(\pm 55/0_6)_s$ laminate as a homogeneous orthotropic laminate is given by the unfilled circular symbol. This homogenized version has a critical stress that is approximately 11% lower than the $(\pm 55/0_6)_s$ laminate, and both laminates have an effective axial modulus equal to 1.96 times the effective modulus of the corresponding quasi-isotropic laminate. However, a homogeneous orthotropic laminate with 68% 0-degree plies and 32% 45-degree plies, indicated

by the unfilled square symbol, has the same critical stress as the $(\pm55/0_6)_s$ laminate and is only 6% less stiff. In addition, the homogenized laminate is only 3% heavier than the optimized laminate of reference 23.

An extensive number of laminate constructions were examined in the present study to determine the merit of representing laminates by their corresponding homogeneous, orthotropic configurations. This effort revealed that the only lay-ups that exceed the critical stress of the corresponding homogenized laminate are those such as the $(\pm55/0_6)_s$ laminate of reference 23 that consist of many unidirectional plies "sandwiched" between a few outside angle plies. Although these sandwich laminates provide slightly higher buckling resistance, high concentrations of plies with the same orientation are likely to result in unacceptable interlaminar shear stresses.

Bending boundary layer attenuation lengths. The buckling analysis presented herein presumes the existence of a uniform, membrane stress state prior to buckling. However, zones of bending stresses occur near the cylinder ends, where radial displacement is constrained, and the extent of these zones is known to depend on laminate orthotropy (see reference 31). The distance from the end of a cylinder to a point along the cylinder generator where the magnitude of the bending stresses has attenuated to a prescribed value is referred to herein as the bending boundary layer attenuation length. The presumption of a membrane prebuckling stress state is typically justified when the bending boundary layer attenuation length is "relatively small" compared to the cylinder length. Thus, having an estimate of the attenuation length associated with a design provides the designer with an indicator of when a more refined buckling analysis may be needed.

Results that show the nondimensional attenuation length of the bending boundary layer are presented in figures 35-37 for values of 0%, 10%, and 50% 90-degree plies, respectively. These attenuation lengths were computed by using equation (48) and are based on a 90% response attenuation tolerance. Several curves are shown in each figure that correspond to values of the percentage of 0-degree plies that range from 10% to 80% 0-degree plies. The solid horizontal red line shown in each figure corresponds to the nondimensional attenuation length of the corresponding quasi-isotropic laminate. The unfilled circular symbols in figure 35 and 37 correspond to (0/±60) and (0/90) laminates, respectively. The filled symbol on figure 35 corresponds to the $(\pm55/0_6)_s$ laminate of reference 23 and its homogenized counterpart. The results for each of these three figures show a monotonic reduction in the attenuation length as the fiber angle increases from 0 to 90 degrees. In addition, each figure generally exhibits a reduction in the attenuation length as the percentage of 0-degree plies diminishes. Furthermore, a reduction in the attenuation length is shown in these three figures as the percentage of 90-degree plies increases.

Concluding Remarks

Simple formulas for the buckling stress of homogeneous, specially orthotropic, laminated-composite cylinders have been presented that are the counterpart of the classical buckling formula for an isotropic cylinder. The formulas were obtained by using nondimensional parameters and equations that facilitate general validation. Numerous results have been presented that establish

the ranges of the nondimensional parameters and coefficients for homogeneous specially orthotropic laminated composites that consist of three families of plies. These three families are 0-degree, 90-degree, and $\pm\theta$ angle plies. Numerous results have also been presented that validate the simple formulas against the exact solution for a wide range of cylinder geometries and laminate constructions. The validation process was greatly simplified by establishing a parametric relationship between the parameters used in the analysis that give the membrane-orthotropy parameter in terms of the flexural-orthotropy parameter. A formula for the buckling stress has been given as a product of a nondimensional coefficient, that involves only material properties of the wall, with the thickness-to-radius ratio of the cylinder and the effective modulus of the corresponding quasi-isotropic laminate. Unlike the corresponding isotropic-cylinder solution, that is represented by a single equation, two equations that depend on the laminate orthotropy were found to be needed to obtain the orthotropic-cylinder solution; one for axisymmetric and one for asymmetric buckling modes.

General results, given in terms of the nondimensional parameters used herein, have also been presented that encompass a wide range of geometries and laminate constructions. These general results also illustrate a wide spectrum of behavioral trends associated with variations in cylinder thinness, aspect ratio, and orthotropy. Design-oriented results have also been presented that provide a simple, clear indication of laminate composition on critical stress, critical strain, and axial stiffness. A very useful graphical form of these results has been presented that enables rapid trade studies for different design requirements. One conclusion found in the present study is that no buckling stress can be achieved for homogeneous specially orthotropic cylinders that is greater than the corresponding quasi-isotropic layup. Another conclusion is that the greater values of buckling stress that can be achieved through tailoring are associated with higher values of axial strain. An example has been provided that demonstrates the application of these results to thin-walled column designs that involve axial stiffness of the cylinder in addition to local buckling.

References

1. Switzky, H.; and Cary, J. W.: Minimum Weight Design of Cylindrical Structures. *AIAA Journal*, vol. 1, no. 10, 1963, pp. 2330-2337.

2. Crawford, R. F.; and Burns, A. B.: Minimum Weight Potentials for Stiffened Plates and Shells. *AIAA Journal*, vol. 1, no. 4, 1963, pp. 879-886.

3. Cohen, G. A.: Optimum Design of Truss-Core Sandwich Cylinders Under Axial Compression. *AIAA Journal*, vol. 1, no. 7, 1963, pp. 1626-1630.

4. Dow, N. F.; and Rosen, B. W.: Structural Efficiency of Orthotropic Cylindrical Shells Subjected to Axial Compression. *AIAA Journal*, vol.4, no. 3, 1966, pp. 481-485.

5. Burns, A. B.; and Almroth, B. O.: Structural Optimization of Axially Compressed, Ring-Stringer Stiffened Cylinders. *Journal of Spacecraft & Rockets*, vol. 3, no. 1, 1966, pp. 19-25.

6. Anon.: *Buckling of Thin-Walled Circular Cylinders*. NASA Space Vehicle Design Criteria, NASA SP-8007, September 1965, revised August 1968.

7. Almroth, B. O.; Burns, A. B.; and Pittner, E. V.: Design Criteria for Axially Loaded Cylindrical Shells. *Journal of Spacecraft & Rockets*, vol. 7, no. 6, 1970, pp. 714-720.

8. Lakshmikantham, C.; and Gerard, G.: Minimum Weight Design of Stiffened Cylinders. *The Aeronautical Quarterly*, February, 1970, pp. 49-68.

9. Tennyson, R. C.; Muggeridge, D. B.; and Caswell, R. D.: New Design Criteria for Predicting Buckling of Cylindrical Shells under Axial Compression. *Journal of Spacecraft & Rockets*, vol. 8, no. 10, 1971, pp. 1062-1067.

10. Tennyson, R. C.; Muggeridge, D. B.; Chan, K. H.; and Khot, N. S.: *Buckling of Fiber-Reinforced Circular Cylinders Under Axial Compression*. Report AFFDL-TR-72-102, Air Force Flight Dynamics Laboratory, August, 1972.

11. Agarwal, B. L.; and Sobel, L. H.: Weight Comparisons of Optimized Stiffened, Unstiffened, and Sandwich Cylindrical Shells. *Journal of Aircraft*, vol. 14, no. 10, 1977, pp. 1000-1008.

12. Almroth, B. O.: *Design of Composite Material Structures for Buckling - An Evaluation of the State-of-the-Art*. Report AFWAL-TR-81-3102, Air Force Flight Dynamics Laboratory, March, 1981.

13. Ershov, N. P.: Stability of Unfigured and Stiffened Shells Made of Fibrous Composites. *Mechanics of Composite Materials*, vol. 4, July-August, 1980, pp. 442-447.

14. Tennyson, R. C.: Thin-Walled Structures in Aerospace Design. *Developments in Thin-Walled Structures - 2*, J. Rhodes and A. C. Walker, eds., Elsevier, 1984, pp. 173-210.

15. Onoda, J.: Optimal Laminate Configurations of Cylindrical Shells for Axial Buckling. *AIAA Journal*, vol. 23, no. 7, 1985, pp. 1093-1098.

16. Moradi, B.; and Parsons, I. D.: Dimensional Analysis of Buckling of Stiffened Composite Shells. *Journal of Engineering Mechanics*, vol. 118, no. 3, 1992, pp. 557-574.

17. Koudela, K. L.; and Strait, L. H.: Simplified Methodology for Prediction of Critical Buckling Pressure for Smooth-Bore Composite Cylindrical Shells. *Journal of Reinforced Plastics and Composites*, vol. 12, May, 1993, pp. 570-583.

18. Zou, R. D.; and Foster, C. G.: Simple Solution for Buckling of Orthotropic Circular Cylindrical Shells. *Thin-Walled Structures*, vol. 22, 1995, pp. 143-158.

19. Xiao, F.; and Li, B.: Study for Critical Values of Collapsing Pressure for Orthotropic Laminated Casing. *Composite Structures*, vol. 32, 1995, pp. 609-614.

20. Weaver, P. M.: Design of Laminated Composite Cylindrical Shells Under Axial Compression. *Composites: Part B*, vol. 31, 2000, pp. 669-679.

21. Weaver, P. M.; Driesen, J. R.; and Roberts, P.: The Effect of Flexural/Twist Anisotropy on Compression Buckling of Quasi-Isotropic Laminated Cylindrical Shells. *Composite Structures*, vol. 55, 2002, pp. 195-204.

22. Weaver, P. M.; Driesen, J. R.; and Roberts, P.: Anisotropic Effects in the Compression Buckling of Laminated Composite Cylindrical Shells. *Composites Science and Technology*, vol. 62, 2002, pp. 91-105.

23. Weaver, P. M.; and Dickenson, R.: Interactive Local/Euler Buckling of Composite Cylindrical Shells. *Computers and Structures*, vol. 81, 2003, pp. 2767-2773.

24. Weaver, P. M.: The Effect of Extension/Twist Anisotropy on Compression Buckling in Cylindrical Shells. *Composites: Part B*, vol. 34, 2003, pp. 251-260.

25. Wong, K. F. W.; Weaver, P. M.; and Jones, D.: A Reduced Solution for Fully Anisotropic Circular Cylindrical Shells Subject to Axial Compression Buckling. *Proceedings of the AIAA/ASME/ASCE/AHS/ASC 46th Structures, Structural Dynamics, and Materials Conference,* 2005, AIAA paper 2005-1868.

26. Wong, K. F. W.; and Weaver, P. M.: Approximate Solution for the Compression Buckling of Fully Anisotropic Cylindrical Shells. *AIAA Journal*, vol. 43, no. 12, 2005, pp. 2639-2645.

27. Weaver, P. M.; and Nemeth, M. P.: Bounds on Flexural Properties and Buckling Response for Symmetrically Laminated Composite Plates. *Journal of Engineering Mechanics*, vol. 133, no. 11, 2007, pp. 1178-1191.

28. Nemeth, M.P.: *Nondimensional Parameters and Equations for Buckling of Symmetrically Laminated Thin Elastic Shallow Shells*. NASA TM 104060, 1991.

29. Jones, R. M.: *Mechanics of Composite Materials*. Second ed., Taylor & Francis, 1999.

30. Jones, R. M.: *Buckling of Bars, Plates, and Shells*. Bull Ridge Publishing, 2006.

31. Nemeth, M. P.; and Smeltzer, S. S., III: *Bending Boundary Layers in Laminated-Composite Circular Cylindrical Shells*. NASA/TP-2000-210549, 2000.

32. Timoshenko, S.: *Strength of Materials - Part II*, Advanced Theory and Problems. Third ed., Krieger Publishing Company, Florida, 1976.

Table 1. Axial half-wavelength, circumferential wave number, and nondimensional load for buckled cylinders with orthotropy parameter $\beta = 0.2$, for selected values of the stiffness-weighted radius-to-thickness ratio ρ (superscripts in parentheses indicate equation numbers)

ρ	$\lambda_{cr}^{(24)}$	$n_{cr}^{(24)}$	$\tilde{p}_{cr}^{(24)}$	$\lambda_{cr}^{(30,\,32c)}$	$n_{cr}^{(31)}$	$\tilde{p}_{cr}^{(32)}$	$\lambda_{cr}^{\infty(33)}$	$n_{cr}^{\infty(33)}$	$\tilde{p}_{cr}^{(34)}$
25	0.250	4	6.60	0.274	3.65	6.50	0.250	4.00	6.60
50	0.200	5	13.02	0.193	5.17	12.99	0.200	5.00	13.02
75	0.167	6	19.60	0.158	6.33	19.49	0.167	6.00	19.60
100	0.143	7	26.08	0.137	7.31	25.98	0.143	7.00	26.08
125	0.125	8	32.51	0.122	8.17	32.48	0.125	8.00	32.51
150	0.111	9	38.98	0.112	8.95	38.97	0.111	9.00	38.98
175	0.100	10	45.57	0.103	9.67	45.47	0.100	10.00	45.57
200	0.100	10	52.08	0.097	10.34	51.97	0.100	10.00	52.08
225	0.091	11	58.46	0.091	10.96	58.46	0.091	11.00	58.46
250	0.083	12	65.14	0.087	11.56	64.96	0.083	12.00	65.14
275	0.083	12	71.47	0.083	12.12	71.45	0.083	12.00	71.47
300	0.077	13	78.06	0.079	12.66	77.95	0.077	13.00	78.06
325	0.077	13	84.47	0.076	13.18	84.44	0.077	13.00	84.47
350	0.071	14	91.04	0.073	13.67	90.94	0.071	14.00	91.04
375	0.071	14	97.46	0.071	14.15	97.44	0.071	14.00	97.46
400	0.067	15	104.07	0.068	14.62	103.93	0.067	15.00	104.07
425	0.067	15	110.43	0.066	15.07	110.43	0.067	15.00	110.43
450	0.063	16	117.16	0.064	15.51	116.92	0.063	16.00	117.15
475	0.063	16	123.43	0.063	15.93	123.42	0.063	16.00	123.42
500	0.063	16	130.04	0.061	16.34	129.91	0.063	16.00	130.03

Table 2. Axial half-wavelength, circumferential wave number, and nondimensional load for buckled cylinders with orthotropy parameter $\beta = 0.5$, for selected values of the stiffness-weighted radius-to-thickness ratio ρ (superscripts in parentheses indicate equation numbers)

ρ	$\lambda_{cr}^{(24)}$	$n_{cr}^{(24)}$	$\tilde{p}_{cr}^{(24)}$	$\lambda_{cr}^{(30,\,32c)}$	$n_{cr}^{(31)}$	$\tilde{p}_{cr}^{(32)}$	$\lambda_{cr}^{\infty(33)}$	$n_{cr}^{\infty(33)}$	$\tilde{p}_{cr}^{(34)}$
25	0.250	4	11.13	0.235	4.26	11.04	0.250	4.00	11.13
50	0.167	6	22.08	0.166	6.03	22.07	0.167	6.00	22.08
75	0.143	7	33.30	0.135	7.38	33.11	0.143	7.00	33.30
100	0.111	9	44.41	0.117	8.52	44.15	0.111	9.00	44.41
125	0.100	10	55.44	0.105	9.53	55.19	0.100	10.00	55.44
150	0.100	10	66.47	0.096	10.44	66.22	0.100	10.00	66.47
175	0.091	11	77.35	0.089	11.27	77.26	0.091	11.00	77.35
200	0.083	12	88.30	0.083	12.05	88.30	0.083	12.00	88.30
225	0.077	13	99.39	0.078	12.78	99.33	0.077	13.00	99.39
250	0.077	13	110.66	0.074	13.47	110.37	0.077	13.00	110.66
275	0.071	14	121.43	0.071	14.13	121.41	0.071	14.00	121.43
300	0.067	15	132.52	0.068	14.76	132.45	0.067	15.00	132.52
325	0.067	15	143.65	0.065	15.36	143.48	0.067	15.00	143.65
350	0.063	16	154.53	0.063	15.94	154.52	0.063	16.00	154.52
375	0.059	17	165.85	0.061	16.50	165.56	0.059	17.00	165.85
400	0.059	17	176.60	0.059	17.04	176.60	0.059	17.00	176.60
425	0.056	18	187.86	0.057	17.57	187.63	0.056	18.00	187.85
450	0.056	18	198.68	0.055	18.08	198.67	0.056	18.00	198.68
475	0.053	19	209.93	0.054	18.57	209.71	0.053	19.00	209.92
500	0.053	19	220.75	0.052	19.06	220.74	0.053	19.00	220.75

Table 3. Axial half-wavelength, circumferential wave number, and nondimensional load for buckled cylinders with orthotropy parameter $\beta = 0.75$, for selected values of the stiffness-weighted radius-to-thickness ratio ρ (superscripts in parentheses indicate equation numbers)

ρ	$\lambda_{cr}^{(24)}$	$n_{cr}^{(24)}$	$\tilde{p}_{cr}^{(24)}$	$\lambda_{cr}^{(30,\,32c)}$	$n_{cr}^{(31)}$	$\tilde{p}_{cr}^{(32)}$	$\lambda_{cr}^{\infty(33)}$	$n_{cr}^{\infty(33)}$	$\tilde{p}_{cr}^{(34)}$
25	0.200	5	14.64	0.223	4.49	14.31	0.250	4.00	14.69
50	0.167	6	28.80	0.157	6.35	28.61	0.167	6.00	28.80
75	0.125	8	42.99	0.129	7.78	42.92	0.125	8.00	42.99
100	0.111	9	57.23	0.111	8.98	57.23	0.111	9.00	57.23
125	0.100	10	71.54	0.100	10.04	71.53	0.100	10.00	71.54
150	0.091	11	85.84	0.091	11.00	85.84	0.091	11.00	85.84
175	0.083	12	100.17	0.084	11.88	100.15	0.083	12.00	100.16
200	0.077	13	114.57	0.079	12.70	114.45	0.077	13.00	114.57
225	0.077	13	129.09	0.074	13.47	128.76	0.077	13.00	129.09
250	0.071	14	143.13	0.070	14.20	143.07	0.071	14.00	143.12
275	0.067	15	157.39	0.067	14.90	157.37	0.067	15.00	157.39
300	0.063	16	171.95	0.064	15.56	171.68	0.063	16.00	171.95
325	0.063	16	186.04	0.062	16.19	185.98	0.063	16.00	186.04
350	0.059	17	200.34	0.060	16.80	200.29	0.059	17.00	200.34
375	0.059	17	214.82	0.057	17.39	214.60	0.059	17.00	214.82
400	0.056	18	228.91	0.056	17.97	228.90	0.056	18.00	228.91
425	0.053	19	243.53	0.054	18.52	243.21	0.053	19.00	243.53
450	0.053	19	257.52	0.052	19.05	257.52	0.053	19.00	257.52
475	0.050	20	272.07	0.051	19.58	271.82	0.050	20.00	272.07
500	0.050	20	286.14	0.050	20.09	286.13	0.050	20.00	286.14

Table 4. Axial half-wavelength, circumferential wave number, and nondimensional load for buckled cylinders with orthotropy parameter $\beta = 1$ (isotropic material), for selected values of the stiffness-weighted radius-to-thickness ratio ρ (superscripts in parentheses indicate equation numbers)

ρ	$\lambda_{cr}^{(24)}$	$n_{cr}^{(24)}$	$\tilde{p}_{cr}^{(24)}$	$\lambda_{cr}^{(30,\,32c)}$	$n_{cr}^{(31)}$	$\tilde{p}_{cr}^{(32)}$	$\lambda_{cr}^{\infty(33)}$	$n_{cr}^{\infty(33)}$	$\tilde{p}_{cr}^{(34)}$
25	0.107	0	17.55	0.107	0.00	17.55	0.107	0.00	17.55
50	0.076	0	35.10	0.076	0.00	35.10	0.076	0.00	35.10
75	0.062	0	52.65	0.062	0.00	52.65	0.062	0.00	52.65
100	0.054	1	70.20	0.054	0.00	70.20	0.054	0.00	70.20
125	0.048	0	87.75	0.048	0.00	87.75	0.048	0.00	87.75
150	0.044	1	105.30	0.044	0.00	105.30	0.044	0.00	105.30
175	0.041	2	122.85	0.041	0.00	122.85	0.041	0.00	122.85
200	0.038	0	140.39	0.038	0.00	140.39	0.038	0.00	140.39
225	0.036	2	157.95	0.036	0.00	157.94	0.036	0.00	157.94
250	0.034	0	175.49	0.034	0.00	175.49	0.034	0.00	175.49
275	1.896	4	193.06	0.032	0.00	193.04	0.032	0.00	193.04
300	0.031	0	210.59	0.031	0.00	210.59	0.031	0.00	210.59
325	0.030	2	228.15	0.030	0.00	228.14	0.030	0.00	228.14
350	0.029	3	245.70	0.029	0.00	245.69	0.029	0.00	245.69
375	0.028	3	263.25	0.028	0.00	263.24	0.028	0.00	263.24
400	0.027	2	280.80	0.027	0.00	280.79	0.027	0.00	280.79
425	0.026	0	298.34	0.026	0.00	298.34	0.026	0.00	298.34
450	2.442	4	315.90	0.025	0.00	315.89	0.025	0.00	315.89
475	2.510	4	333.45	0.025	0.00	333.44	0.025	0.00	333.44
500	0.024	0	350.99	0.024	0.00	350.99	0.024	0.00	350.99

Table 5. Axial half-wavelength, circumferential wave number, and nondimensional load for buckled cylinders with orthotropy parameter $\beta = 1.5$, for selected values of the stiffness-weighted radius-to-thickness ratio ρ (superscripts in parentheses indicate equation numbers)

ρ	$\lambda_{cr}^{(24)}$	$n_{cr}^{(24)}$	$\tilde{p}_{cr}^{(24)}$	$\lambda_{cr}^{(30,\,32c)}$	$n_{cr}^{(31)}$	$\tilde{p}_{cr}^{(32)}$	$\lambda_{cr}^{\infty(33)}$	$n_{cr}^{\infty(33)}$	$\tilde{p}_{cr}^{(34)}$
25	0.107	0	17.55	0.107	0.00	17.55	0.107	0.00	17.55
50	0.076	0	35.10	0.076	0.00	35.10	0.076	0.00	35.10
75	0.062	0	52.65	0.062	0.00	52.65	0.062	0.00	52.65
100	0.054	0	70.20	0.054	0.00	70.20	0.054	0.00	70.20
125	0.048	0	87.75	0.048	0.00	87.75	0.048	0.00	87.75
150	0.044	0	105.30	0.044	0.00	105.30	0.044	0.00	105.30
175	0.041	0	122.85	0.041	0.00	122.85	0.041	0.00	122.85
200	0.038	0	140.39	0.038	0.00	140.39	0.038	0.00	140.39
225	0.036	0	157.94	0.036	0.00	157.94	0.036	0.00	157.94
250	0.034	0	175.49	0.034	0.00	175.49	0.034	0.00	175.49
275	0.032	0	193.04	0.032	0.00	193.04	0.032	0.00	193.04
300	0.031	0	210.59	0.031	0.00	210.59	0.031	0.00	210.59
325	0.030	0	228.14	0.030	0.00	228.14	0.030	0.00	228.14
350	0.029	0	245.69	0.029	0.00	245.69	0.029	0.00	245.69
375	0.028	0	263.24	0.028	0.00	263.24	0.028	0.00	263.24
400	0.027	0	280.79	0.027	0.00	280.79	0.027	0.00	280.79
425	0.026	0	298.34	0.026	0.00	298.34	0.026	0.00	298.34
450	0.025	0	315.89	0.025	0.00	315.89	0.025	0.00	315.89
475	0.025	0	333.44	0.025	0.00	333.44	0.025	0.00	333.44
500	0.024	0	350.99	0.024	0.00	350.99	0.024	0.00	350.99
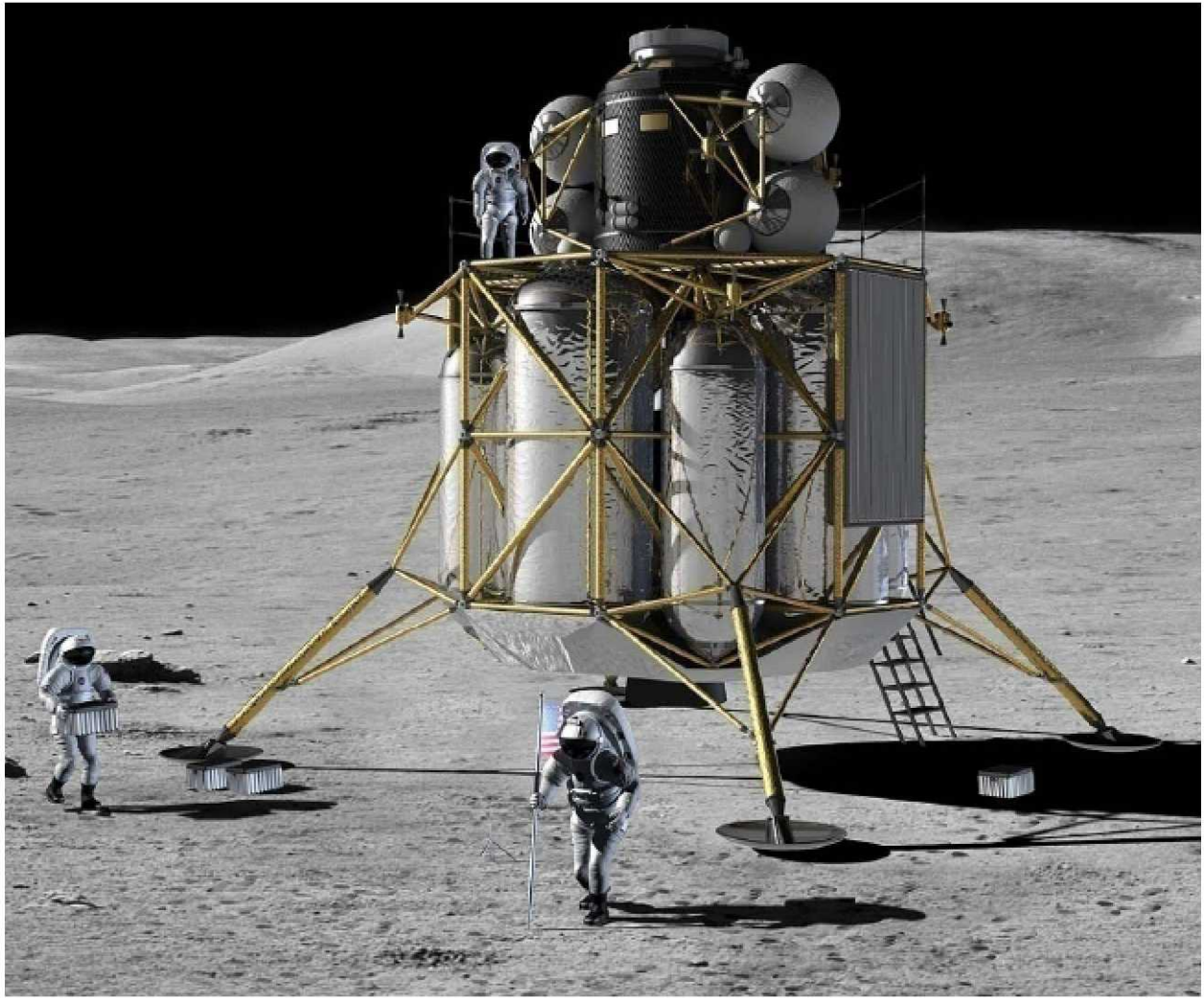
Figure 1. The Altair lunar lander.
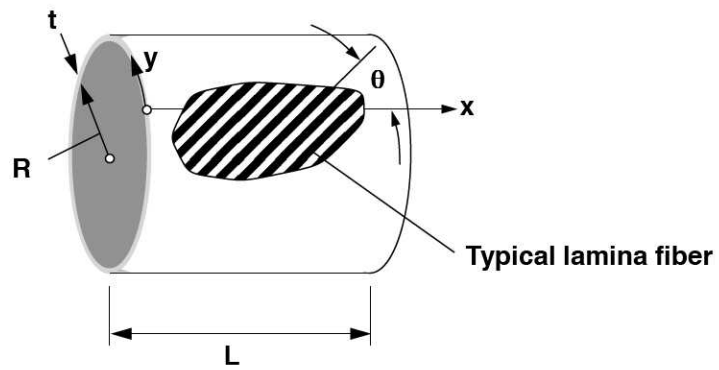
Figure 2. Cylinder geometry, surface coordinate system, and lamina fiber orientation.
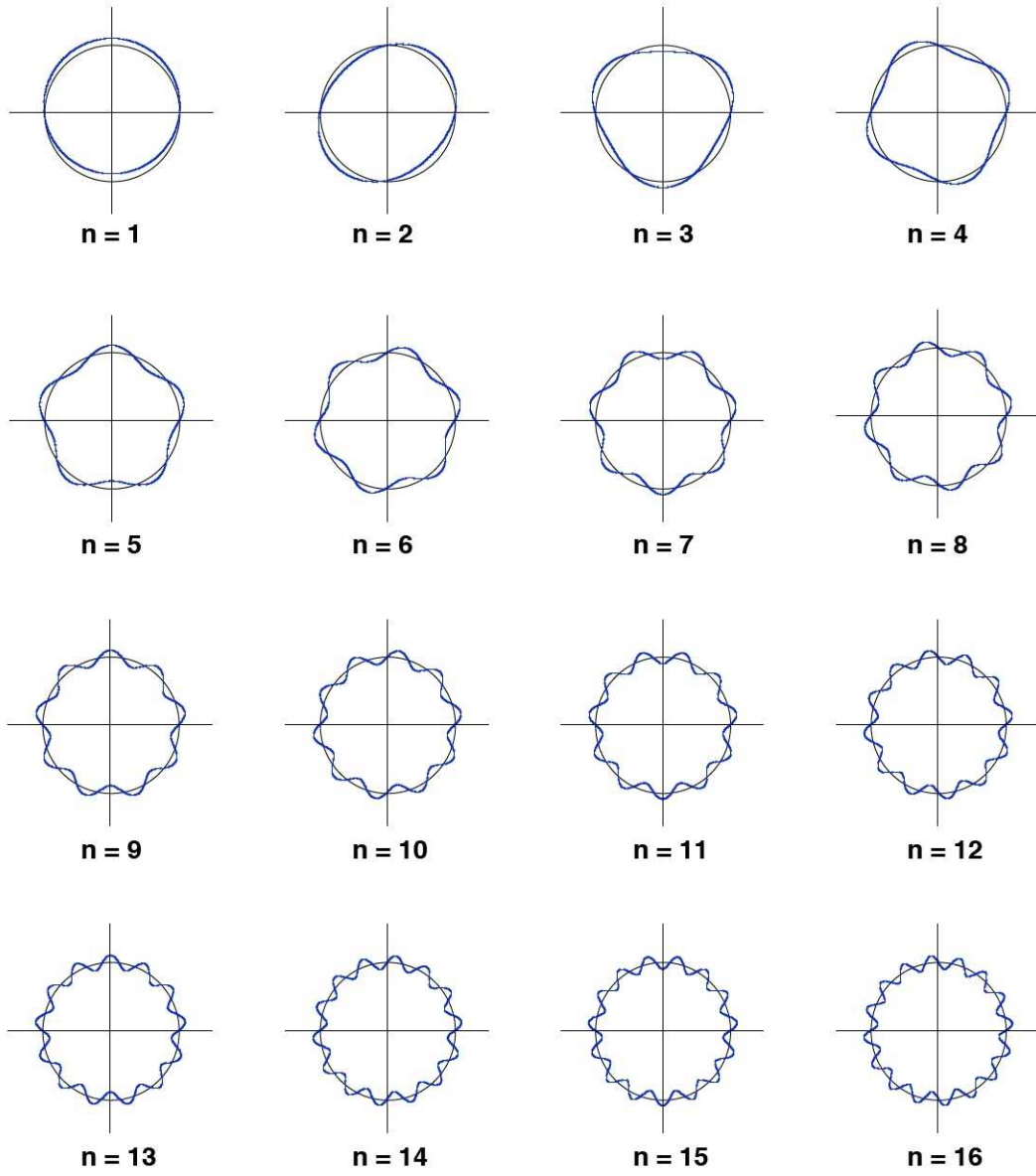
Figure 3. Circumferential waveforms used in equation (12).
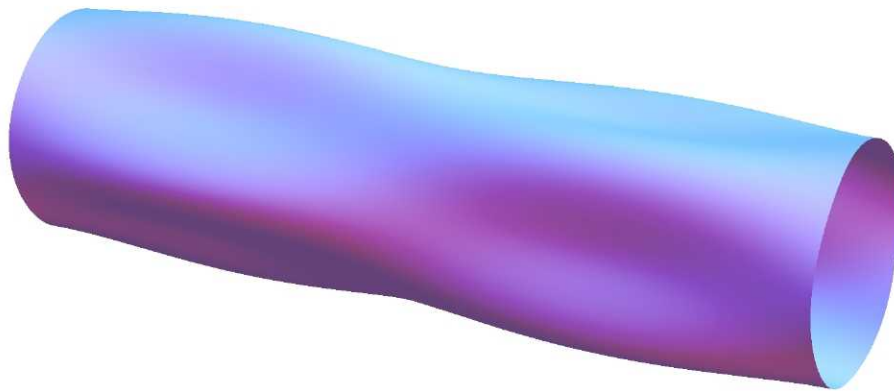
(a) Three-dimensional rendering of a buckling mode

Axial half-wave length

Buckle

$2\pi R$

$m_{cr} = 2$

$n_{cr} = 4$

L
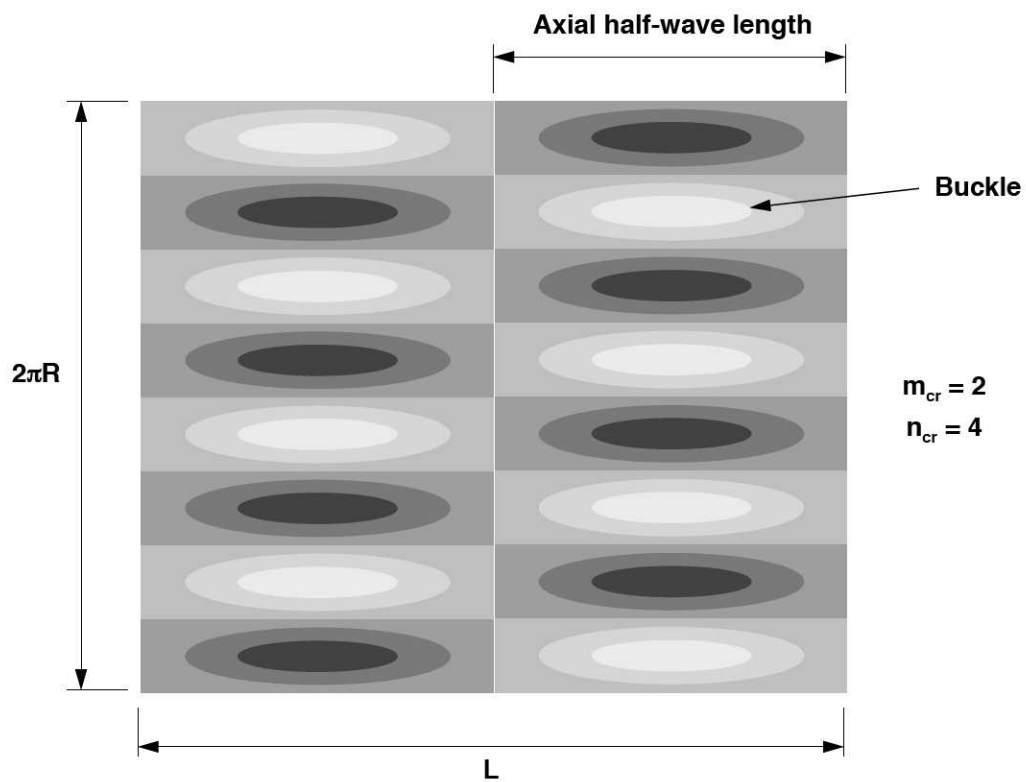
(b) Contour plot of the radial displacement

Figure 4. Typical buckle pattern of a compression-loaded cylinder.

$$\beta = \sqrt{\nu_{xy}\nu_{yx}} + \frac{2G_{xy}}{\sqrt{E_x E_y}}\left(1 - \nu_{xy}\nu_{yx}\right)$$
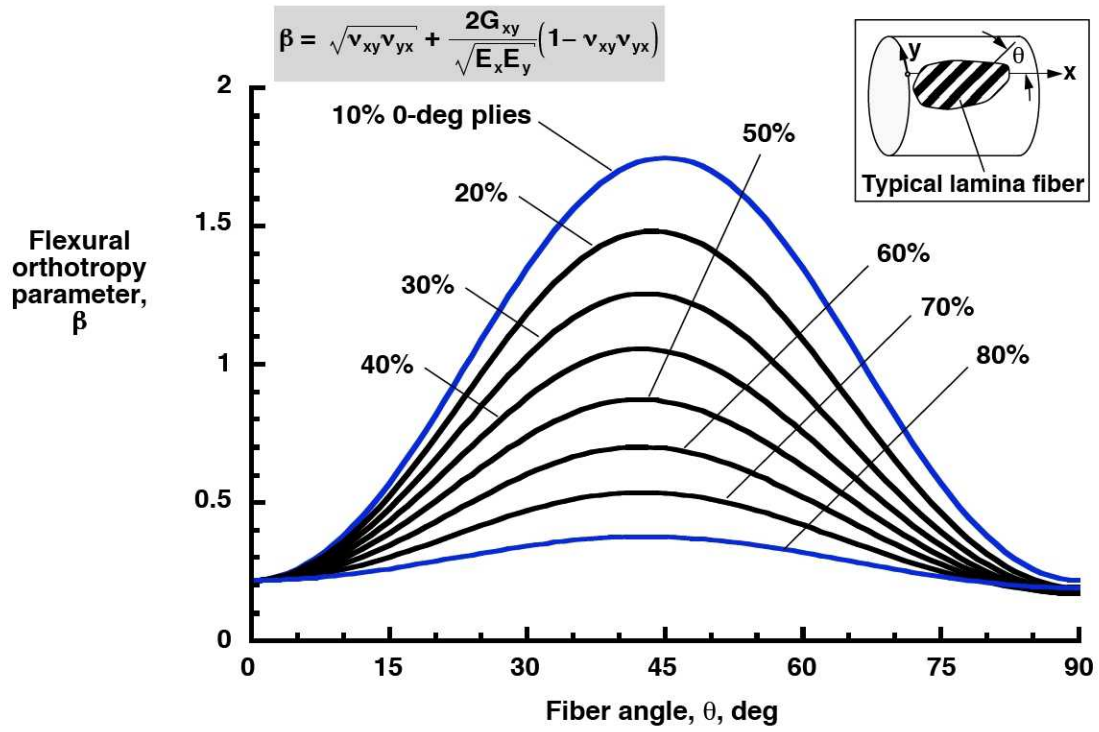
Figure 5. Effects of fiber angle and percentage of 0-degree plies on nondimensional flexural orthotropy parameter β for shell walls with 10% 90-degree plies.

$$\mu = \frac{\sqrt{E_x E_y}}{2G_{xy}} - \sqrt{\nu_{xy}\nu_{yx}}$$
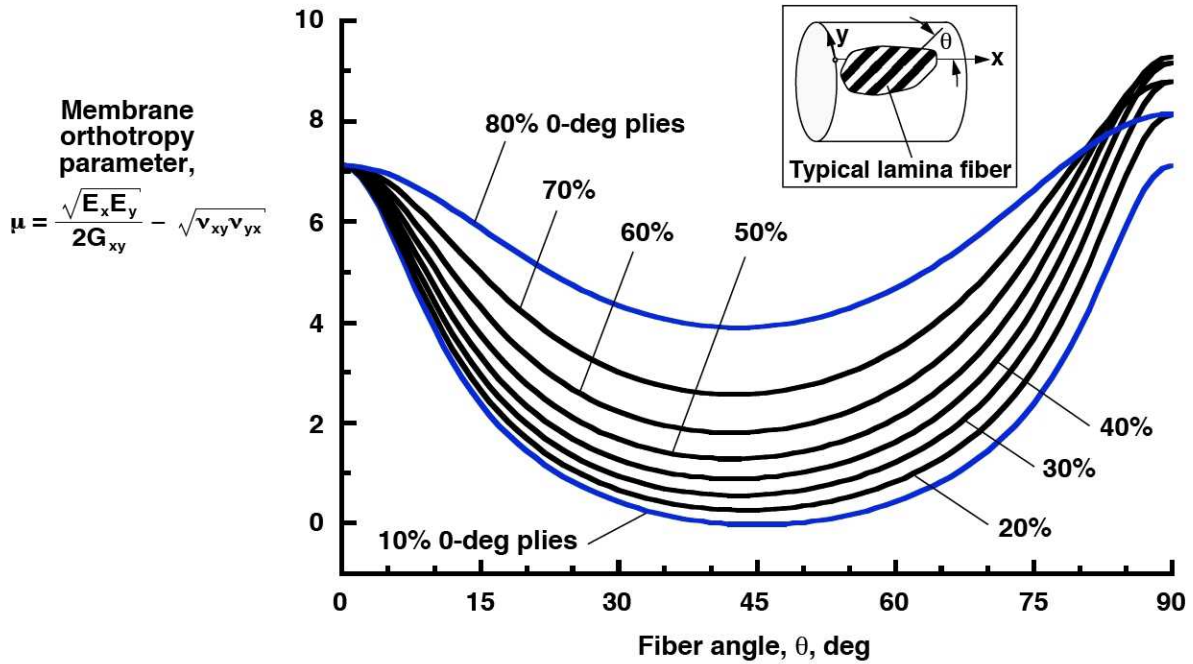
Figure 6. Effects of fiber angle and percentage of 0-degree plies on nondimensional flexural orthotropy parameter μ for shell walls with 10% 90-degree plies.
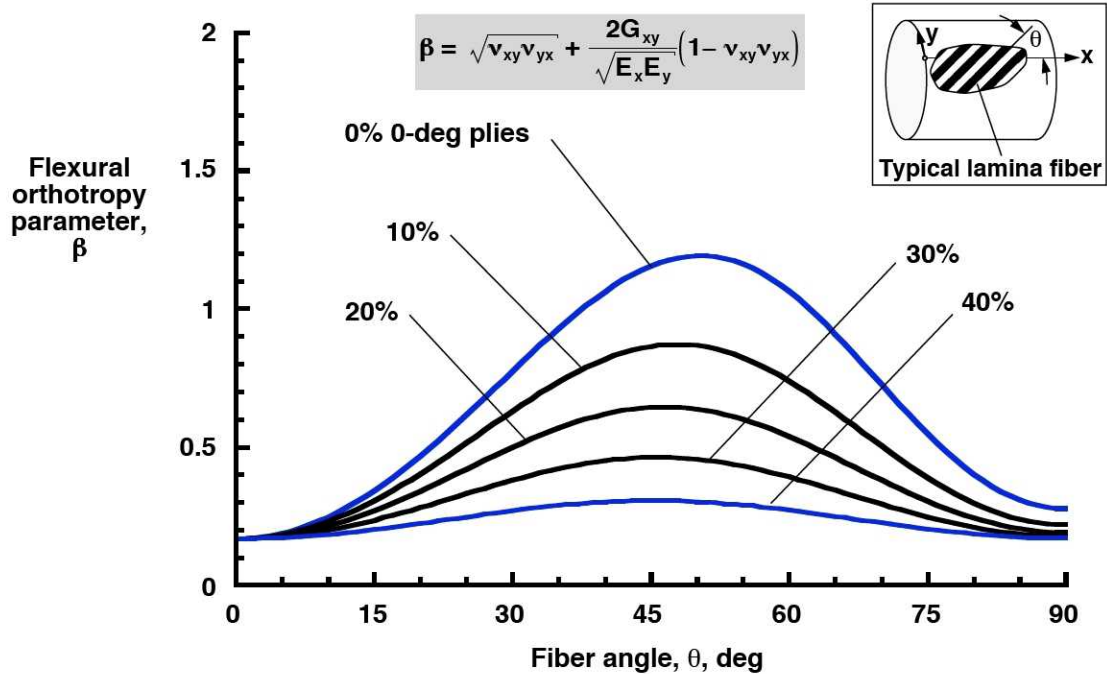
Figure 7. Effects of fiber angle and percentage of 0-degree plies on nondimensional flexural orthotropy parameter β for shell walls with 50% 90-degree plies.
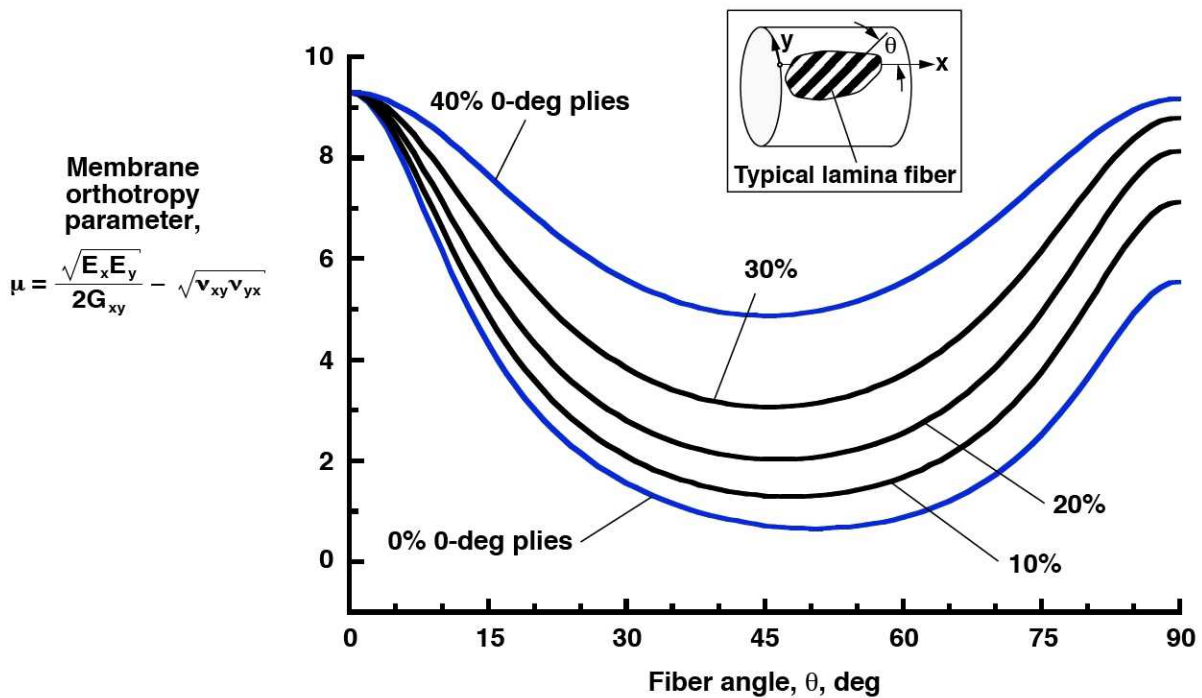
Figure 8. Effects of fiber angle and percentage of 0-degree plies on nondimensional flexural orthotropy parameter μ for shell walls with 50% 90-degree plies.

Membrane orthotropy parameter,

$$\mu = \frac{\sqrt{E_x E_y}}{2G_{xy}} - \sqrt{\nu_{xy} \nu_{yx}}$$

Least squares fit given by Eq. (54)

Flexural orthotropy parameter, $\quad \beta = \sqrt{\nu_{xy} \nu_{yx}} + \frac{2G_{xy}}{\sqrt{E_x E_y}} \left(1 - \nu_{xy} \nu_{yx} \right)$
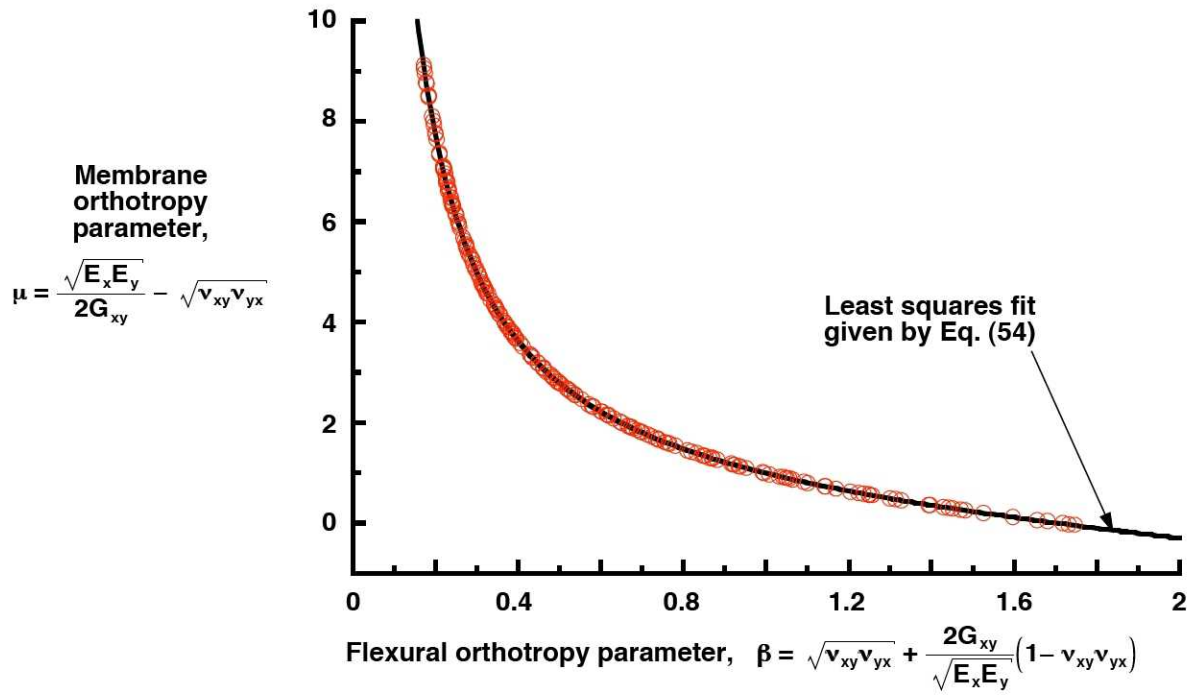
Figure 9. Nondimensional orthotropy parameter μ as a function of the nondimensional orthotropy parameter β for shell walls with any percentage of 0-degree and 90-degree plies and fiber angle.

$$\alpha_m = \frac{L}{R} \left(\frac{E_y}{E_x} \right)^{\frac{1}{4}}$$

Orthotropy coefficient,

$$\left(\frac{E_y}{E_x} \right)^{\frac{1}{4}}$$

20% 30% 40%

10% 0-deg plies

50%

60%

70% 80%

Typical lamina fiber
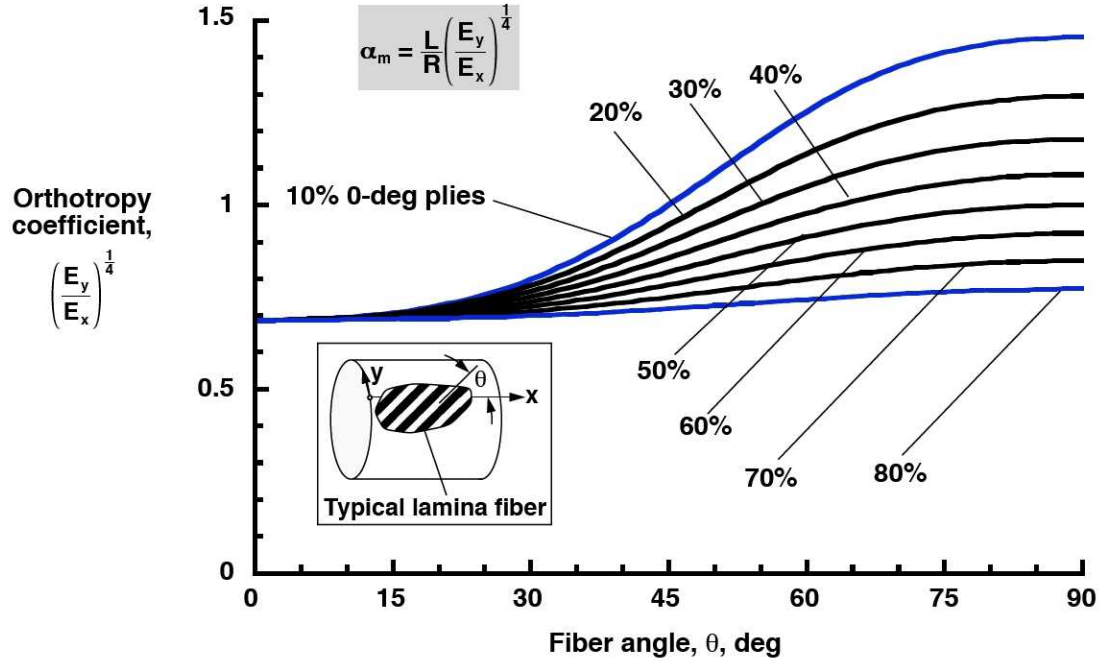
Fiber angle, θ, deg

Figure 10. Effects of fiber angle and percentage of 0-degree plies on nondimensional orthotropy coefficient $(E_y/E_x)^{1/4}$ for shell walls with 10% 90-degree plies.
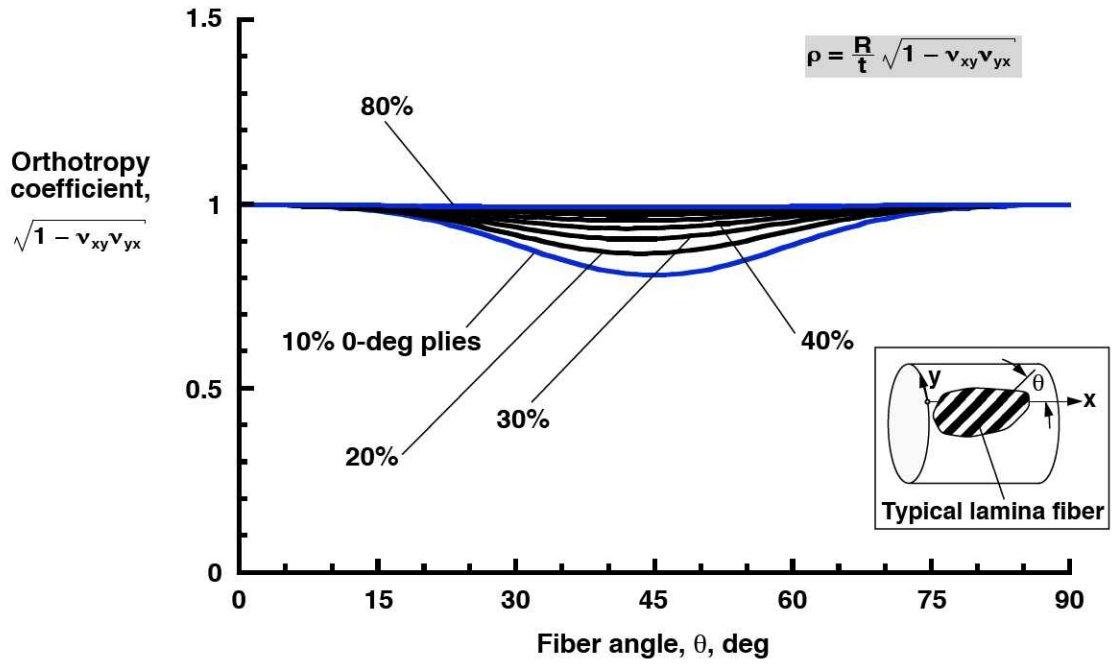
Figure 11. Effects of fiber angle and percentage of 0-deg plies on nondimensional orthotropy coefficient $\sqrt{1 - \nu_{xy}\nu_{yx}}$ for shell walls with 10% 90-degree plies.
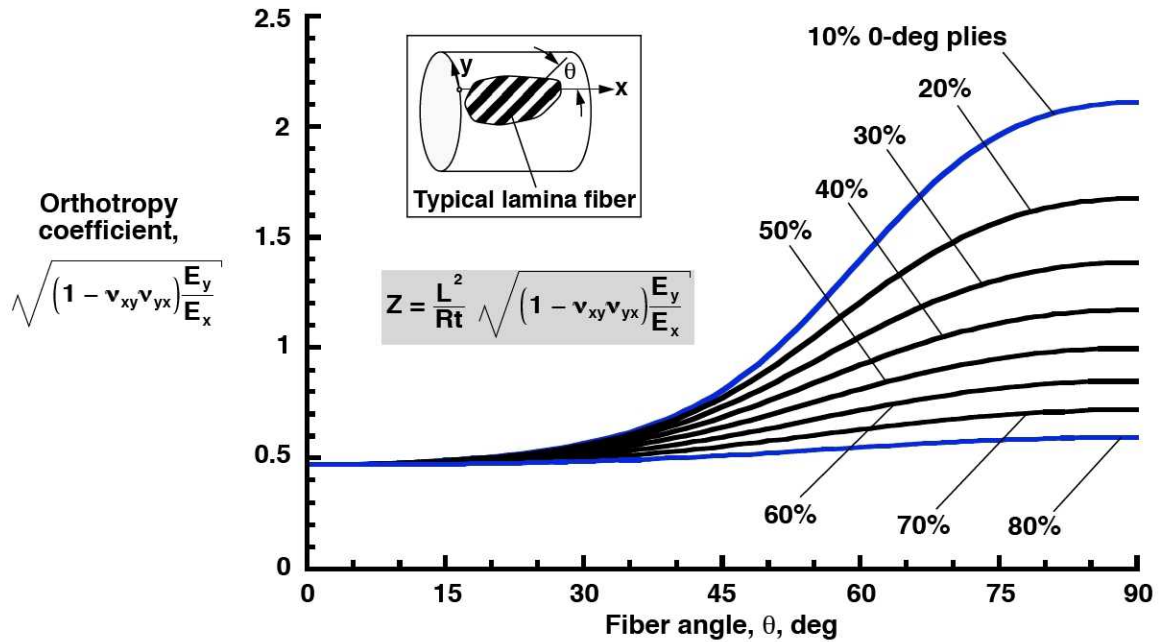
Figure 12. Effects of fiber angle and percentage of 0-degree plies on nondimensional orthotropy coefficient $\sqrt{\left(1 - \nu_{xy}\nu_{yx}\right)\dfrac{E_y}{E_x}}$ for shell walls with 10% 90-degree plies.

37
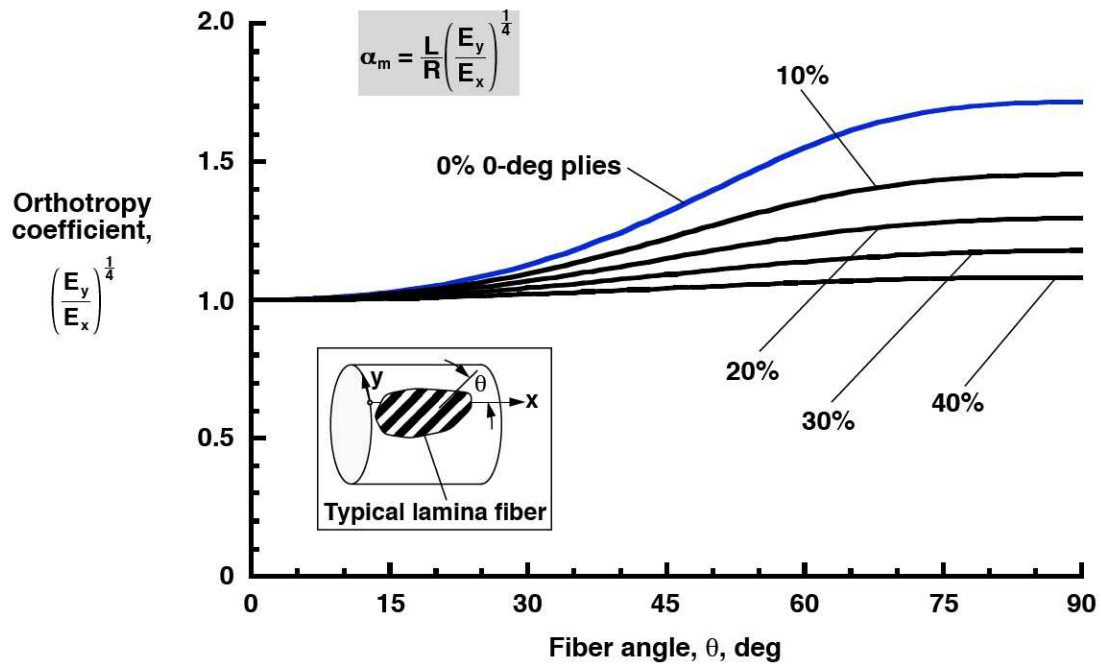
Figure 13. Effects of fiber angle and percentage of 0-degree plies on nondimensional orthotropy coefficient $(E_y/E_x)^{1/4}$ for shell walls with 50% 90-degree plies.
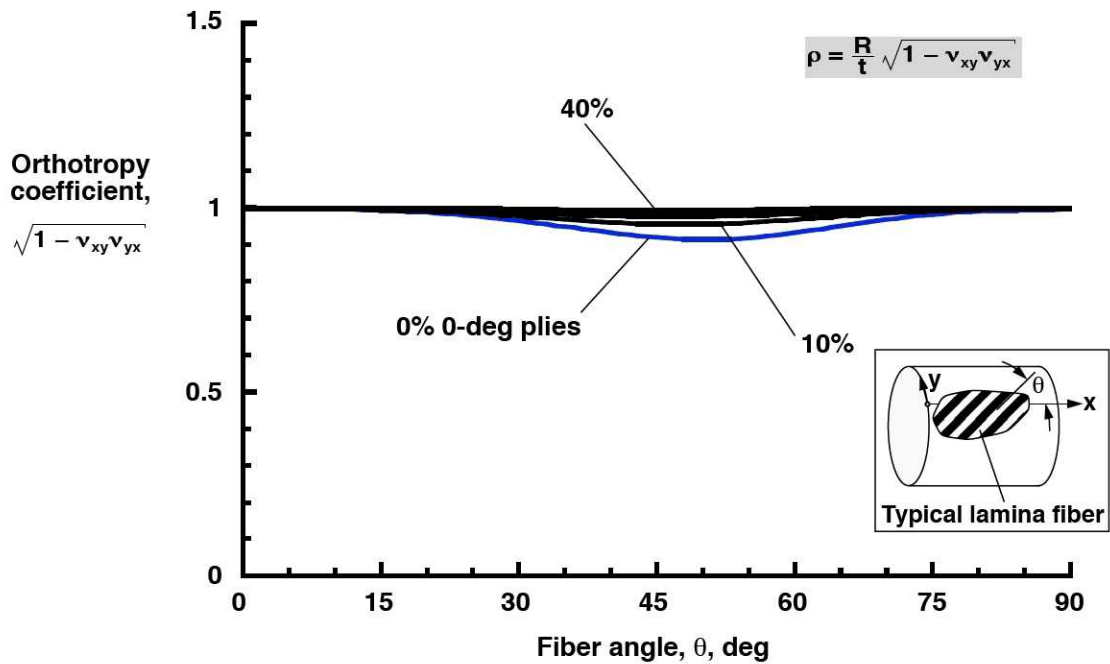
Figure 14. Effects of fiber angle and percentage of 0-degree plies on nondimensional orthotropy coefficient $\sqrt{1 - \nu_{xy}\nu_{yx}}$ for shell walls with 50% 90-degree plies.
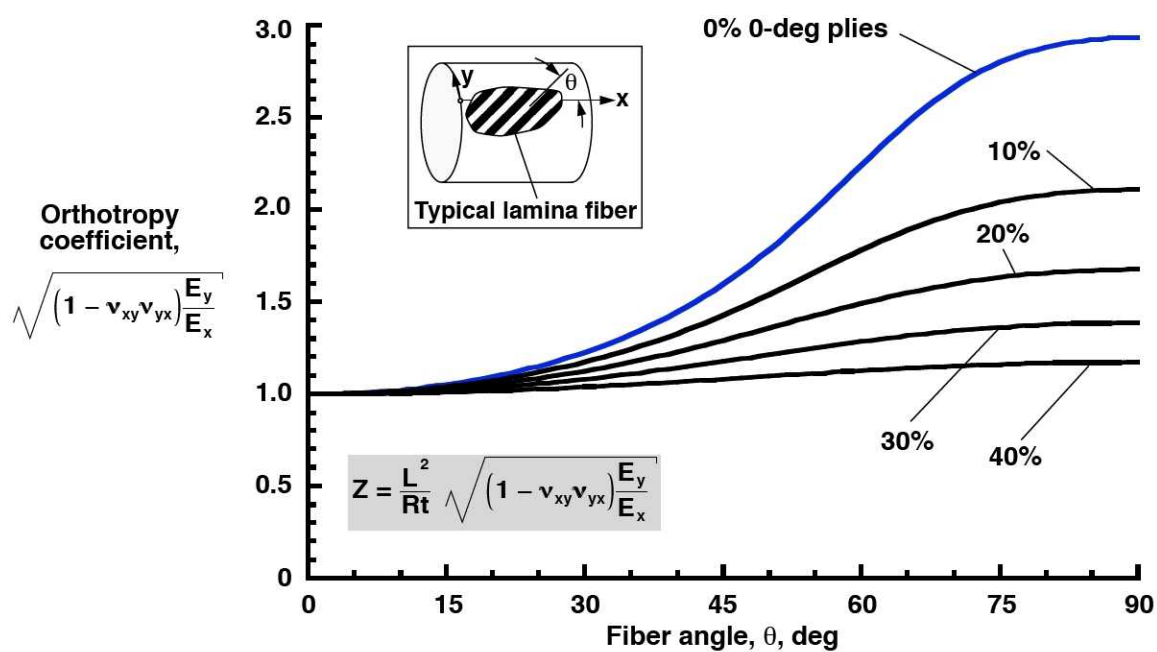
Figure 15. Effects of fiber angle and percentage of 0-degree plies on nondimensional orthotropy coefficient $\sqrt{\left(1 - \nu_{xy}\nu_{yx}\right)\dfrac{E_y}{E_x}}$ **for shell walls with 50% 90-degree plies.**
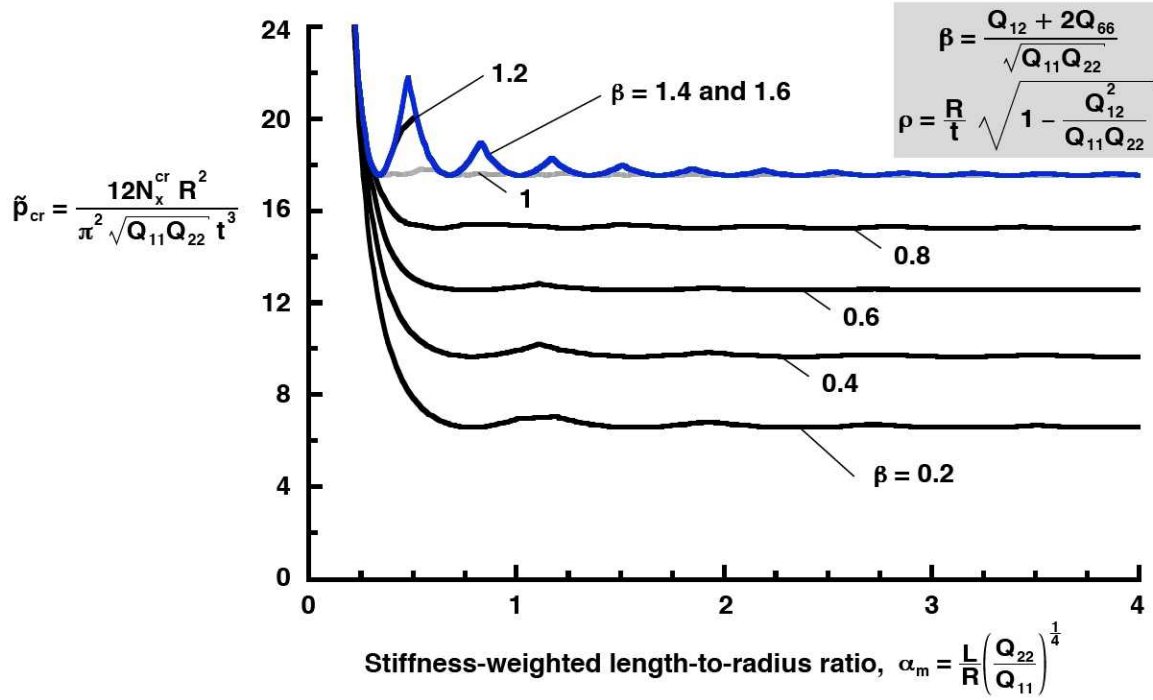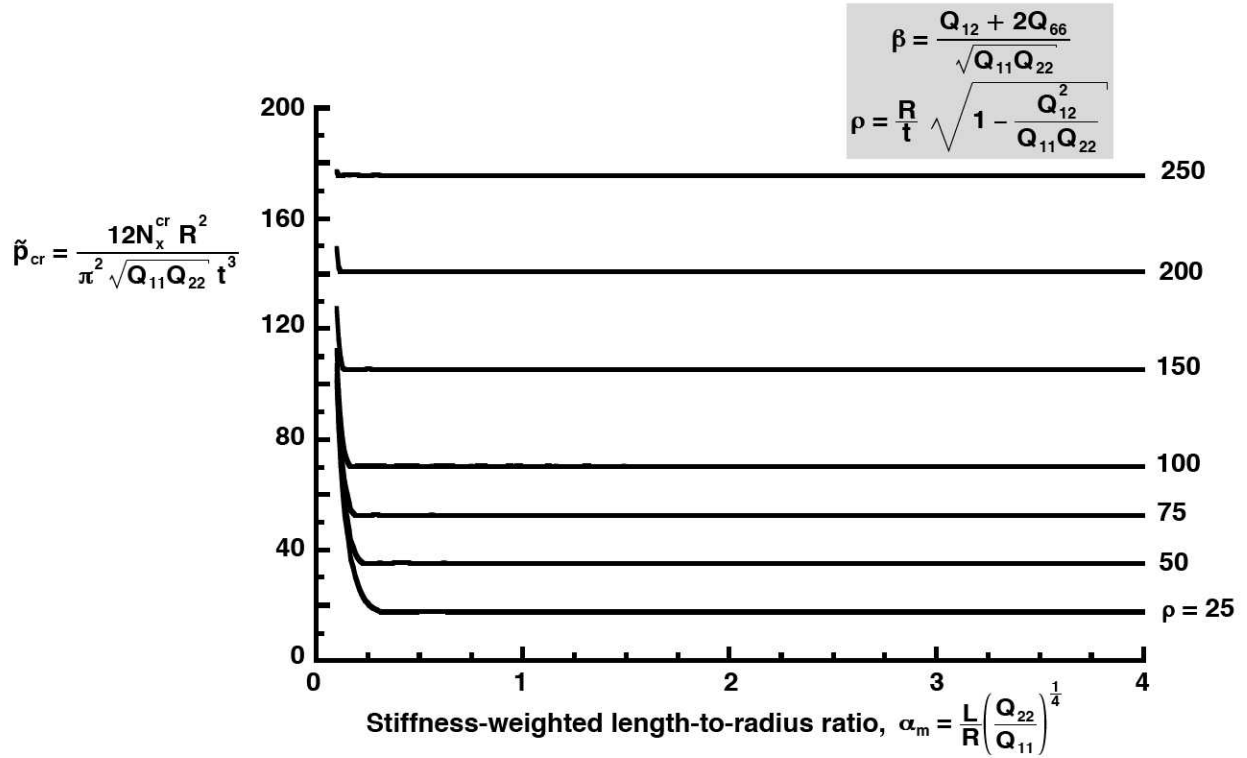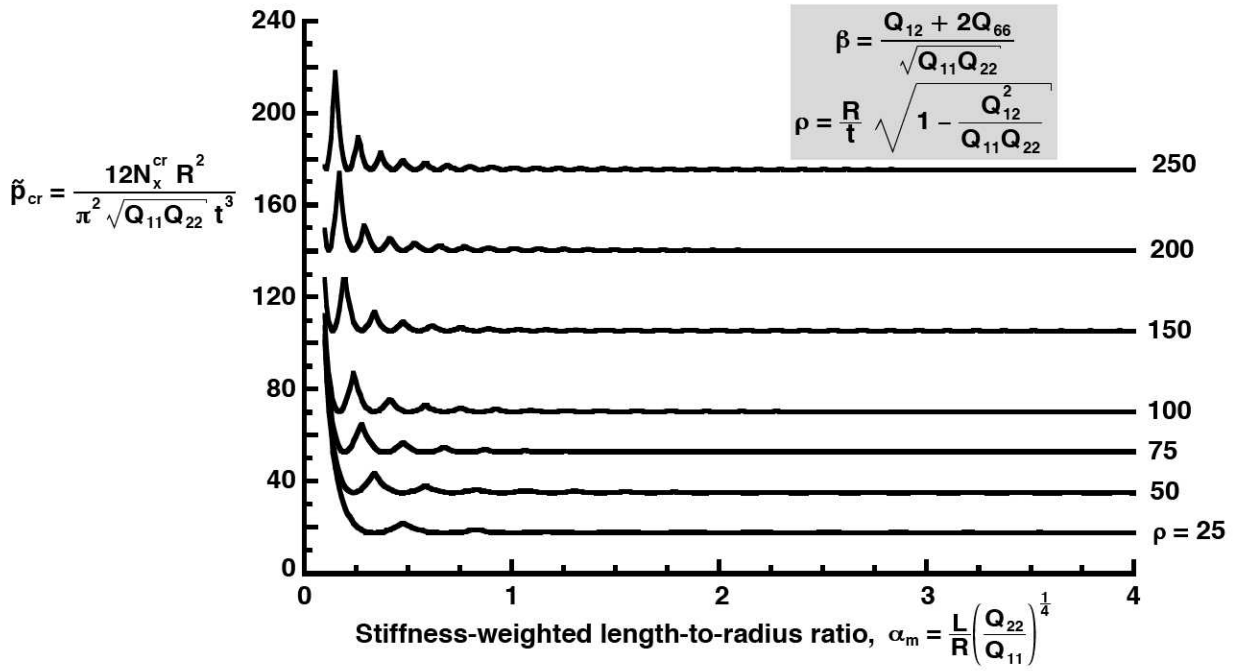
Figure 16. Effects of parameters α_m and β on nondimensional buckling loads on cylinders with nondimensional thinness ratio $\rho = 25$.
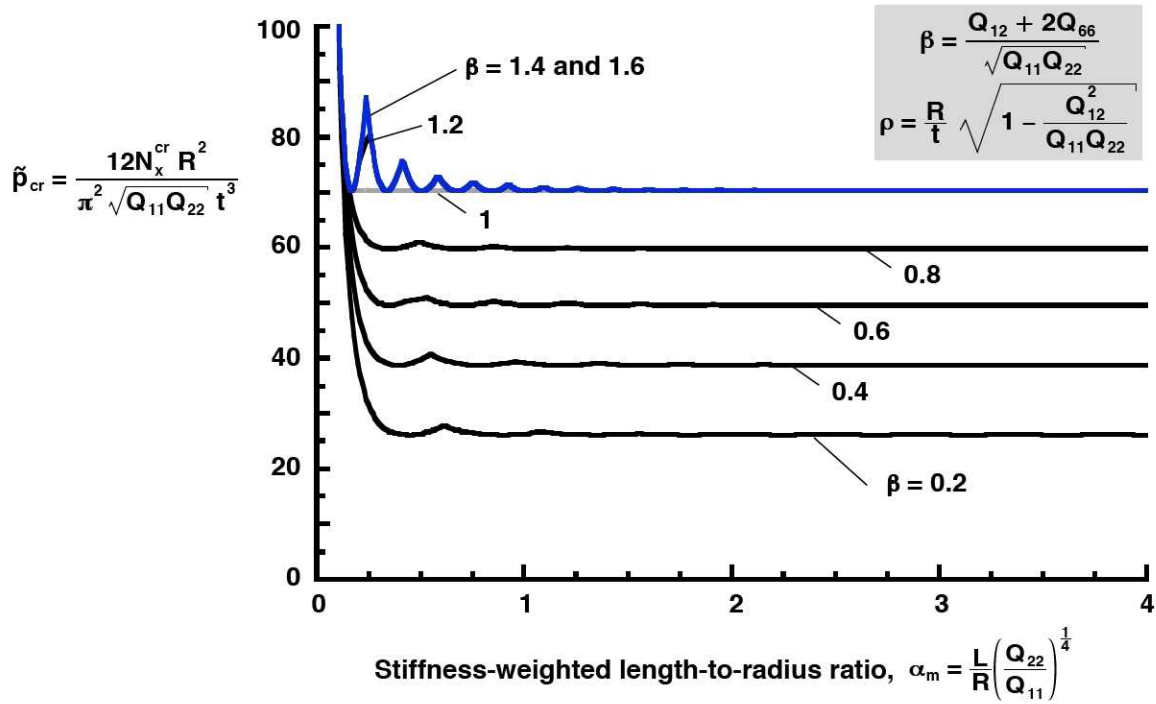
Figure 17. Effects of parameters α_m and β on nondimensional buckling loads on cylinders with nondimensional thinness ratio $\rho = 100$.

$$\tilde{p}_{cr} = \frac{12N_x^{cr} R^2}{\pi^2 \sqrt{Q_{11}Q_{22}}\, t^3}$$

$$\beta = \frac{Q_{12} + 2Q_{66}}{\sqrt{Q_{11}Q_{22}}}$$

$$\rho = \frac{R}{t}\sqrt{1 - \frac{Q_{12}^2}{Q_{11}Q_{22}}}$$

Stiffness-weighted length-to-radius ratio, $\alpha_m = \frac{L}{R}\left(\frac{Q_{22}}{Q_{11}}\right)^{\frac{1}{4}}$
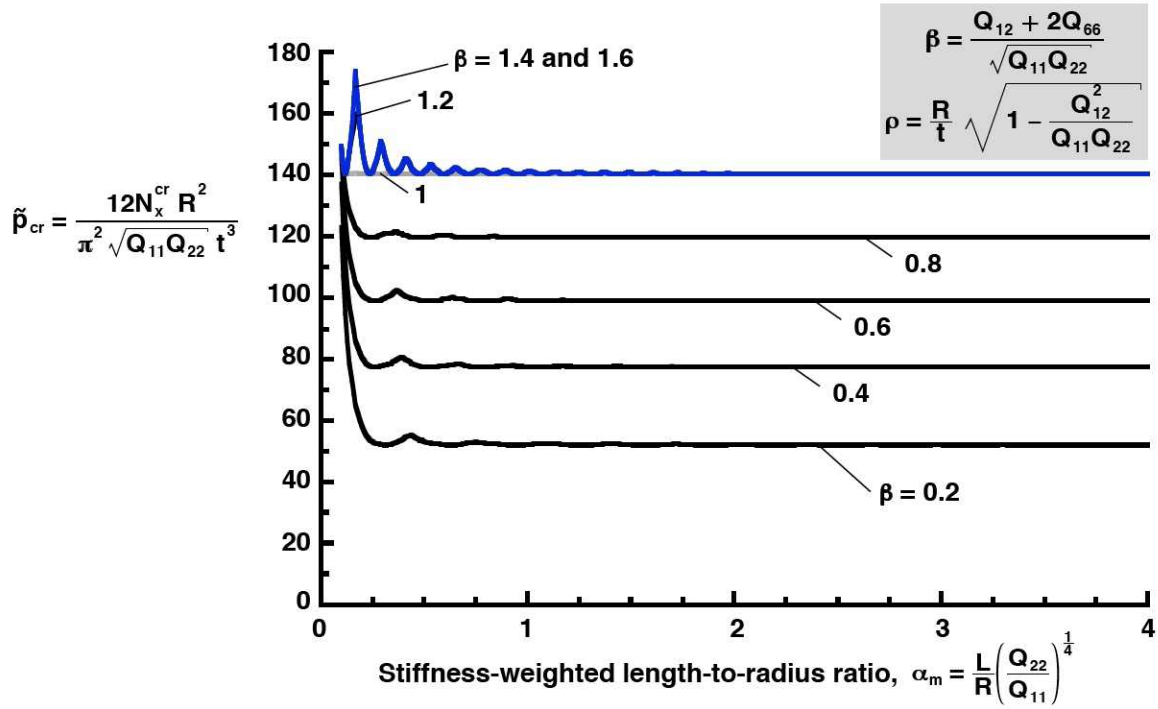
Figure 18. Effects of parameters α_m and β on nondimensional buckling loads on cylinders with nondimensional thinness ratio $\rho = 200$.

$$\tilde{p}_{cr} = \frac{12N_x^{cr} R^2}{\pi^2 \sqrt{Q_{11}Q_{22}}\, t^3}$$

$$\beta = \frac{Q_{12} + 2Q_{66}}{\sqrt{Q_{11}Q_{22}}}$$

$$\rho = \frac{R}{t}\sqrt{1 - \frac{Q_{12}^2}{Q_{11}Q_{22}}}$$

Stiffness-weighted length-to-radius ratio, $\alpha_m = \frac{L}{R}\left(\frac{Q_{22}}{Q_{11}}\right)^{\frac{1}{4}}$
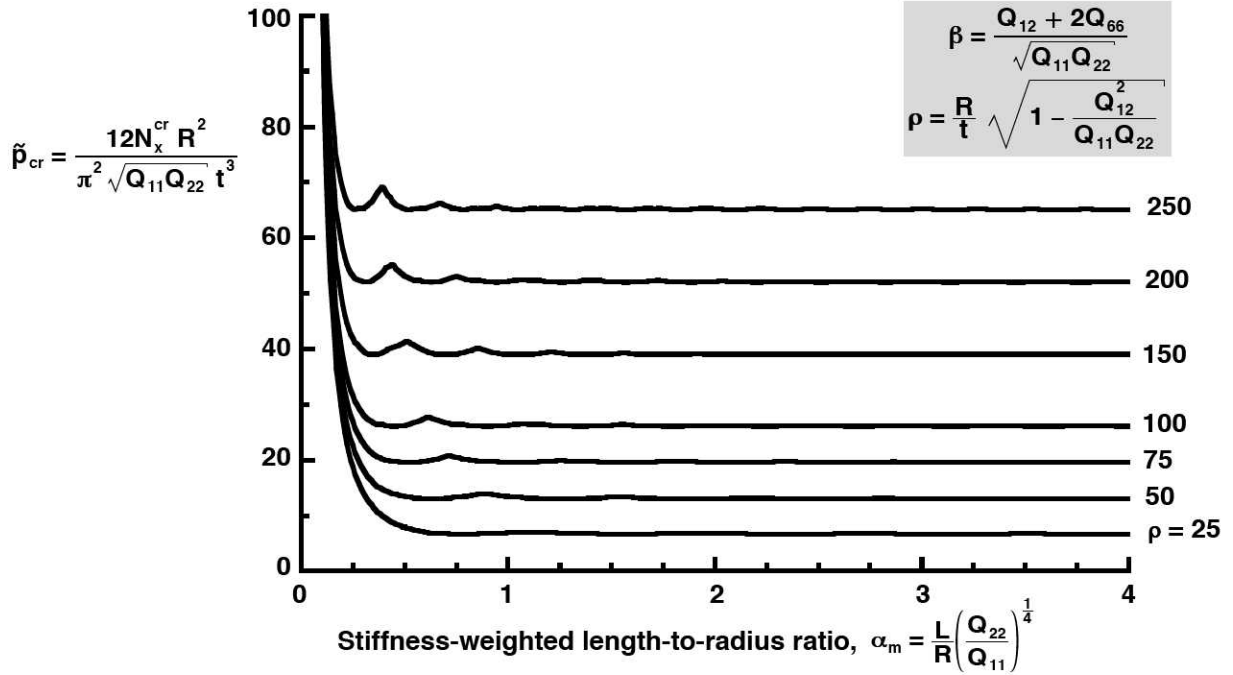
Figure 19. Effects of parameters α_m and ρ on nondimensional buckling loads on cylinders with nondimensional orthotropy parameter $\beta = 0.2$.

$$\tilde{p}_{cr} = \frac{12 N_x^{cr} R^2}{\pi^2 \sqrt{Q_{11}Q_{22}}\, t^3}$$

$$\beta = \frac{Q_{12} + 2Q_{66}}{\sqrt{Q_{11}Q_{22}}}$$

$$\rho = \frac{R}{t} \sqrt{1 - \frac{Q_{12}^2}{Q_{11}Q_{22}}}$$

Stiffness-weighted length-to-radius ratio, $\alpha_m = \dfrac{L}{R}\left(\dfrac{Q_{22}}{Q_{11}}\right)^{\frac{1}{4}}$
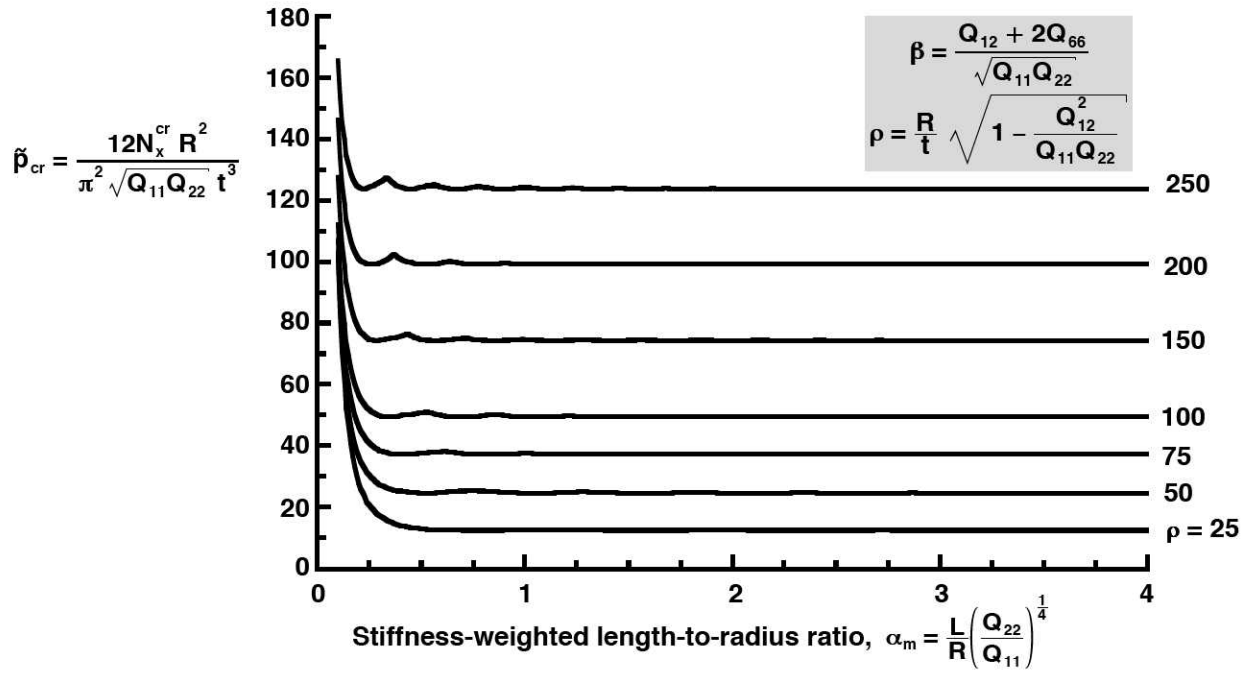
Figure 20. Effects of parameters α_m and ρ on nondimensional buckling loads on cylinders with nondimensional orthotropy parameter $\beta = 0.6$.

$$\beta = \frac{Q_{12} + 2Q_{66}}{\sqrt{Q_{11}Q_{22}}}$$

$$\rho = \frac{R}{t} \sqrt{1 - \frac{Q_{12}^2}{Q_{11}Q_{22}}}$$

$$\tilde{p}_{cr} = \frac{12 N_x^{cr} R^2}{\pi^2 \sqrt{Q_{11}Q_{22}}\, t^3}$$

Stiffness-weighted length-to-radius ratio, $\alpha_m = \dfrac{L}{R}\left(\dfrac{Q_{22}}{Q_{11}}\right)^{\frac{1}{4}}$

Figure 21. Effects of parameters α_m and ρ on nondimensional buckling loads on cylinders with nondimensional orthotropy parameter $\beta = 1$.

$$\tilde{p}_{cr} = \frac{12 N_x^{cr} R^2}{\pi^2 \sqrt{Q_{11} Q_{22}} \ t^3}$$

$$\beta = \frac{Q_{12} + 2Q_{66}}{\sqrt{Q_{11} Q_{22}}}$$

$$\rho = \frac{R}{t} \sqrt{1 - \frac{Q_{12}^2}{Q_{11} Q_{22}}}$$

250

200

150

100

75

50

$\rho = 25$

Stiffness-weighted length-to-radius ratio, $\alpha_m = \dfrac{L}{R} \left(\dfrac{Q_{22}}{Q_{11}} \right)^{\frac{1}{4}}$

Figure 22. Effects of parameters α_m and ρ on nondimensional buckling loads on cylinders with nondimensional orthotropy parameter $\beta = 1.6$.

$$\tilde{p}_{cr} = \frac{12 N_x^{cr} R^2}{\pi^2 \sqrt{Q_{11} Q_{22}} \ t^3}$$

$\tilde{p}_{cr}^{(21)}$

$\tilde{p}_{cr}^{(34)}$

$\tilde{p}_{cr}^{(32)}$

$$\beta = \frac{Q_{12} + 2Q_{66}}{\sqrt{Q_{11} Q_{22}}}$$

$$\rho = \frac{R}{t} \sqrt{1 - \frac{Q_{12}^2}{Q_{11} Q_{22}}}$$

Stiffness-weighted length-to-radius ratio, $\alpha_m = \dfrac{L}{R} \left(\dfrac{Q_{22}}{Q_{11}} \right)^{\frac{1}{4}}$
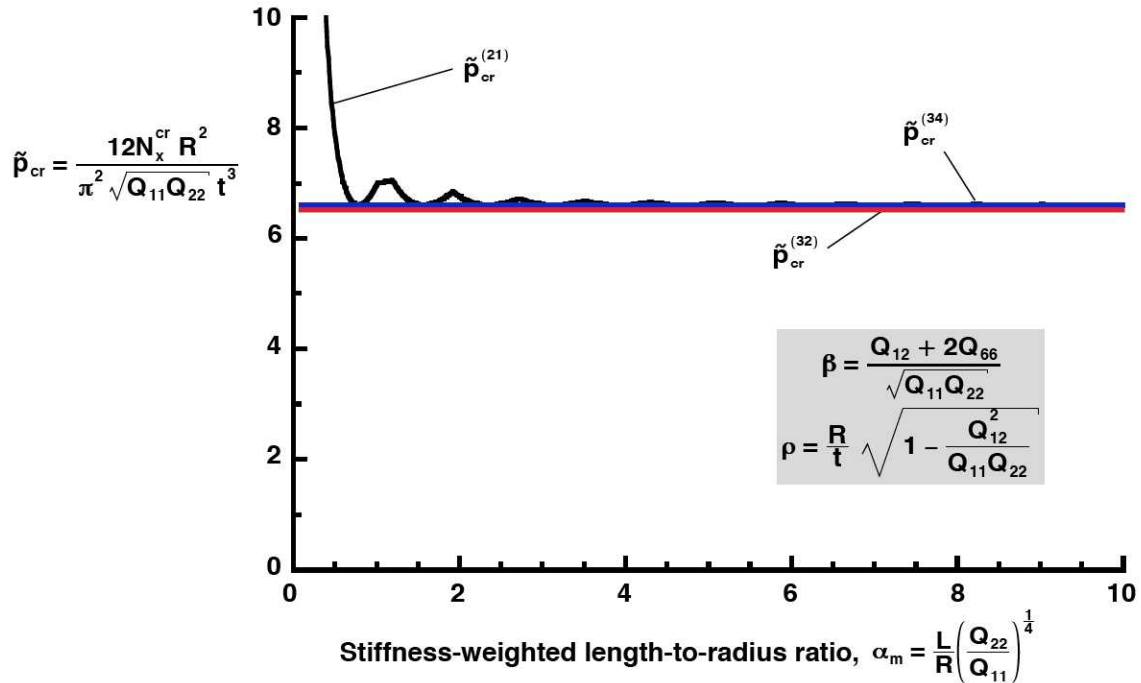
Figure 23. Effect of enforcing periodicity on the accuracy of the nondimensional buckling loads of infinitely long cylinders with $\beta = 0.2$ and $\rho = 25$ (superscripts on the nondimensional buckling loads indicate equation numbers).
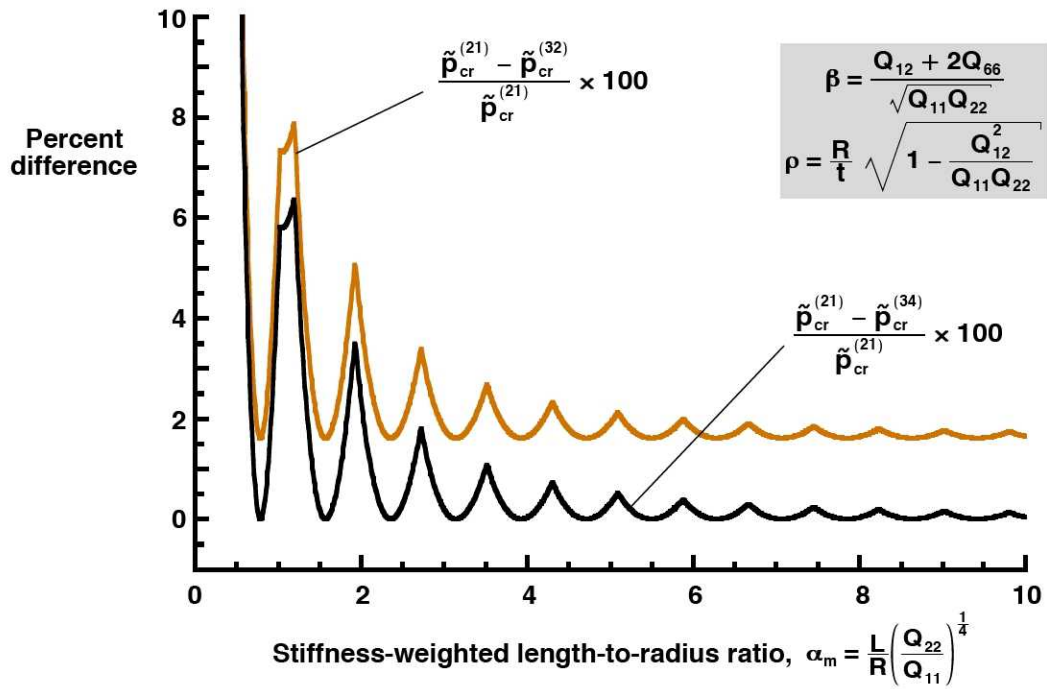
Figure 24. Effect of enforcing periodicity on the accuracy of the nondimensional buckling loads of infinitely long cylinders with β = 0.2 and ρ = 25 (superscripts on the nondimensional buckling loads indicate equation numbers).
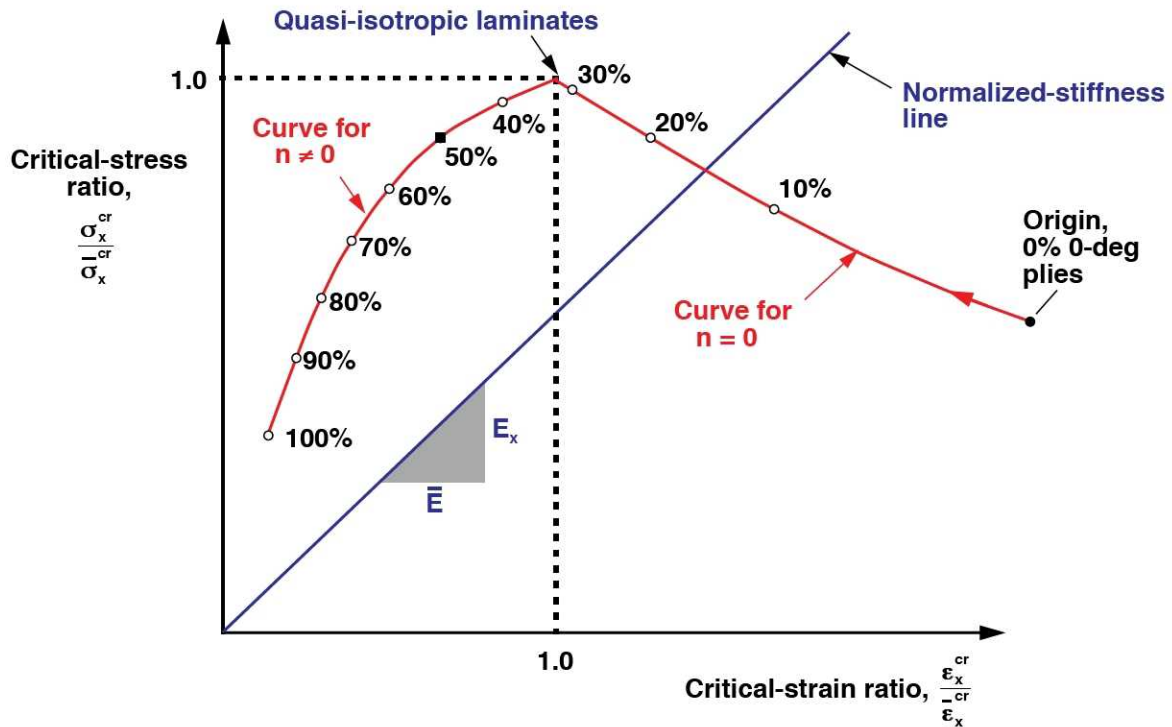
Figure 25. Arc-length coordinate system for the percentage of 0-degree plies used on plots of critical-strain versus critical-stress ratios for shell walls with a fixed fiber angle θ and a fixed percentage of 90-degree plies.
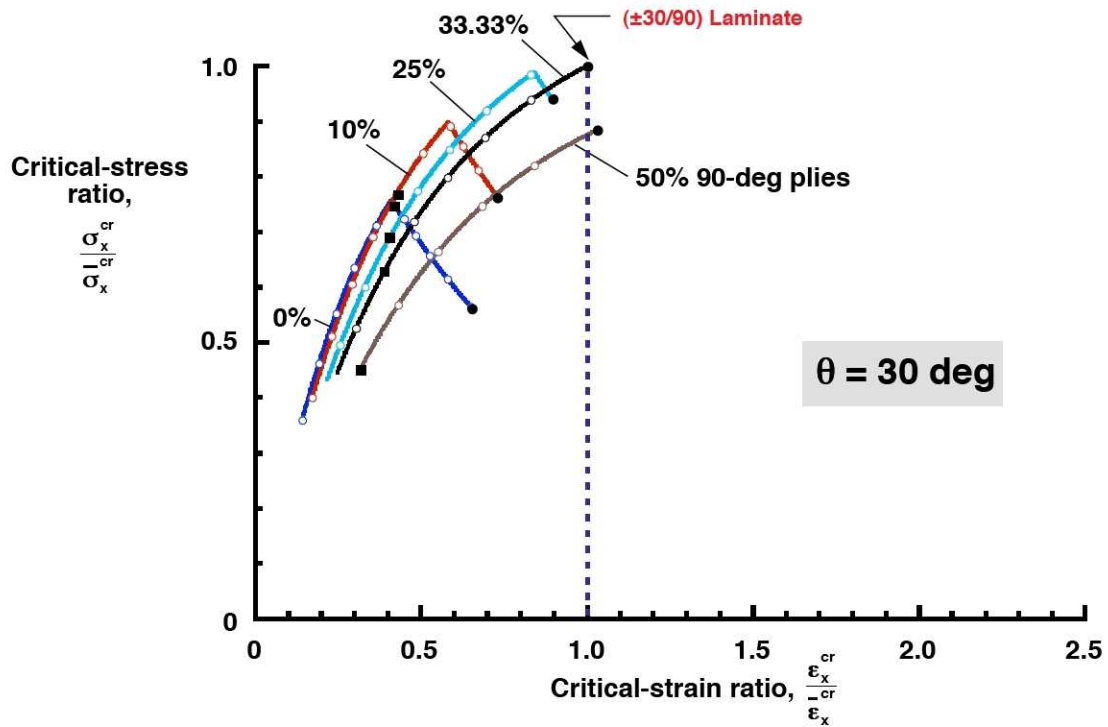
Figure 26. Effects of the percentage of 0-degree and 90-degree plies on the critical-strain and critical-stress ratios for shell walls with a fiber angle θ = 30 degrees.
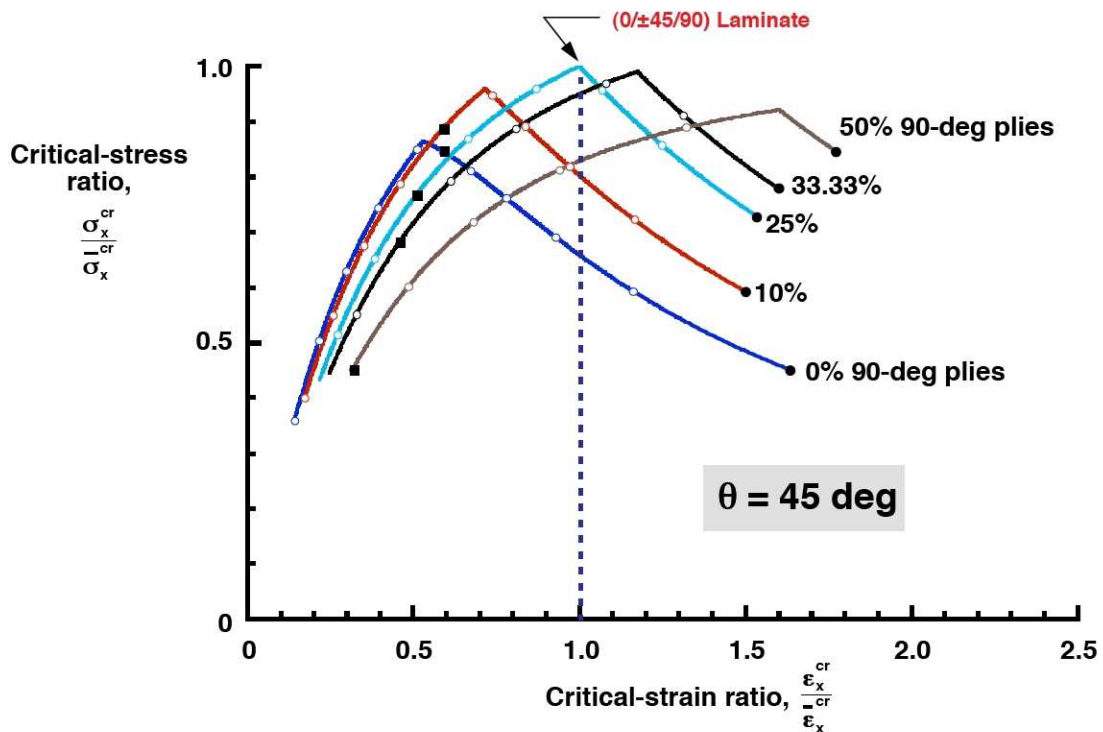
Figure 27. Effects of the percentage of 0-degree and 90-degree plies on the critical-strain and critical-stress ratios for shell walls with a fiber angle θ = 45 degrees.
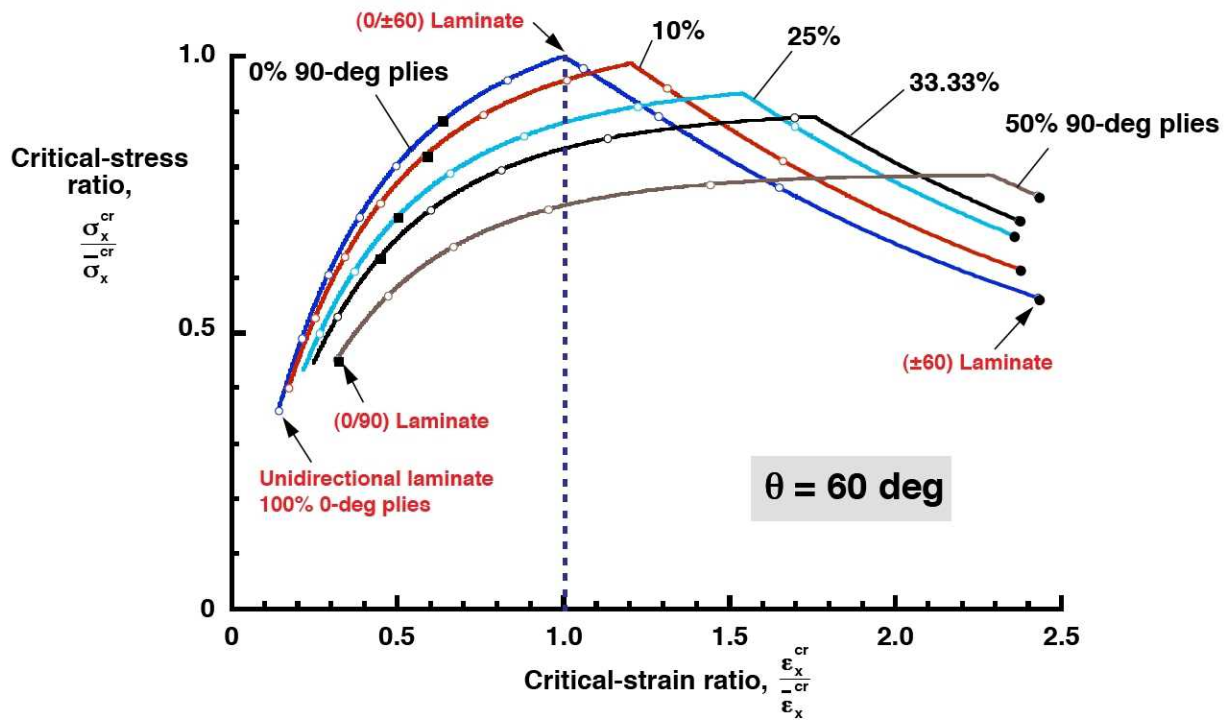
Figure 28. Effects of the percentage of 0-degree and 90-degree plies on the critical-strain and critical-stress ratios for shell walls with a fiber angle $\theta = 60$ degrees.
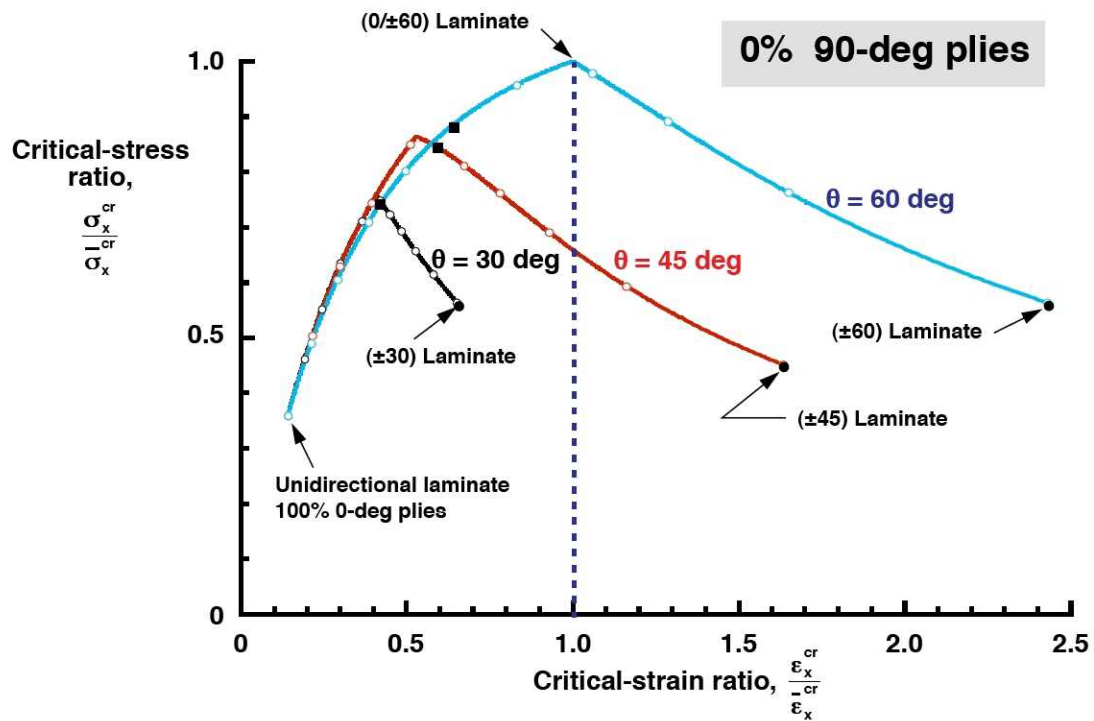
Figure 29. Effects of the fiber angle θ and the percentage of 0-degree plies on the critical-strain and critical-stress ratios for shell walls with no 90-degree plies.
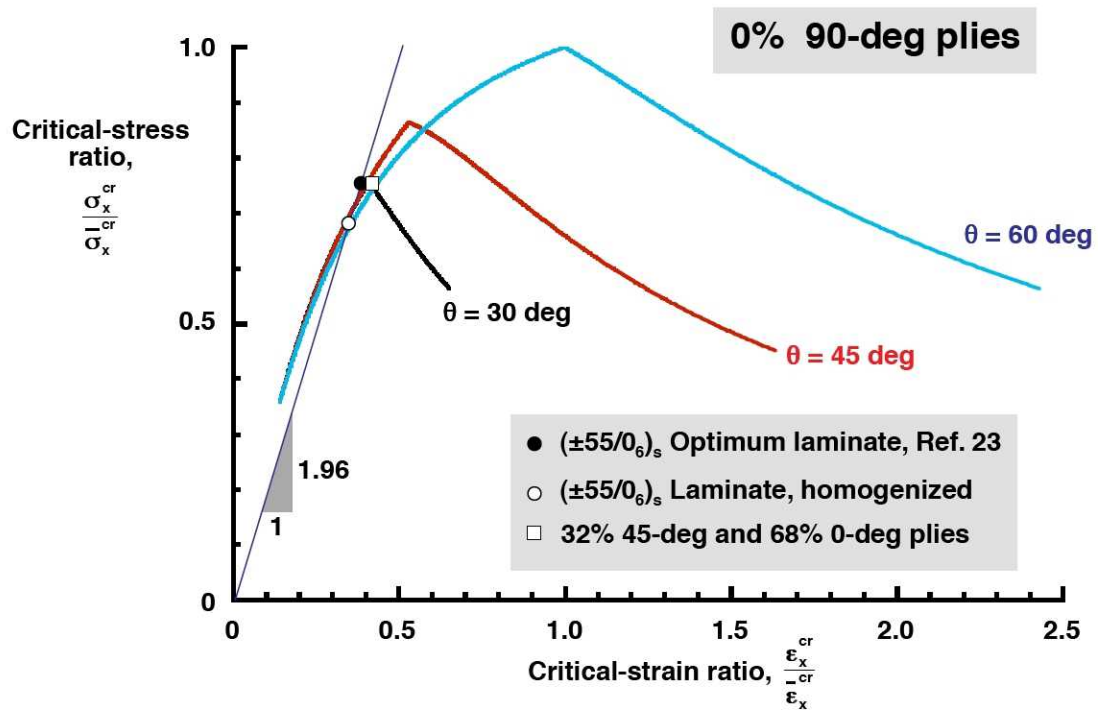
46
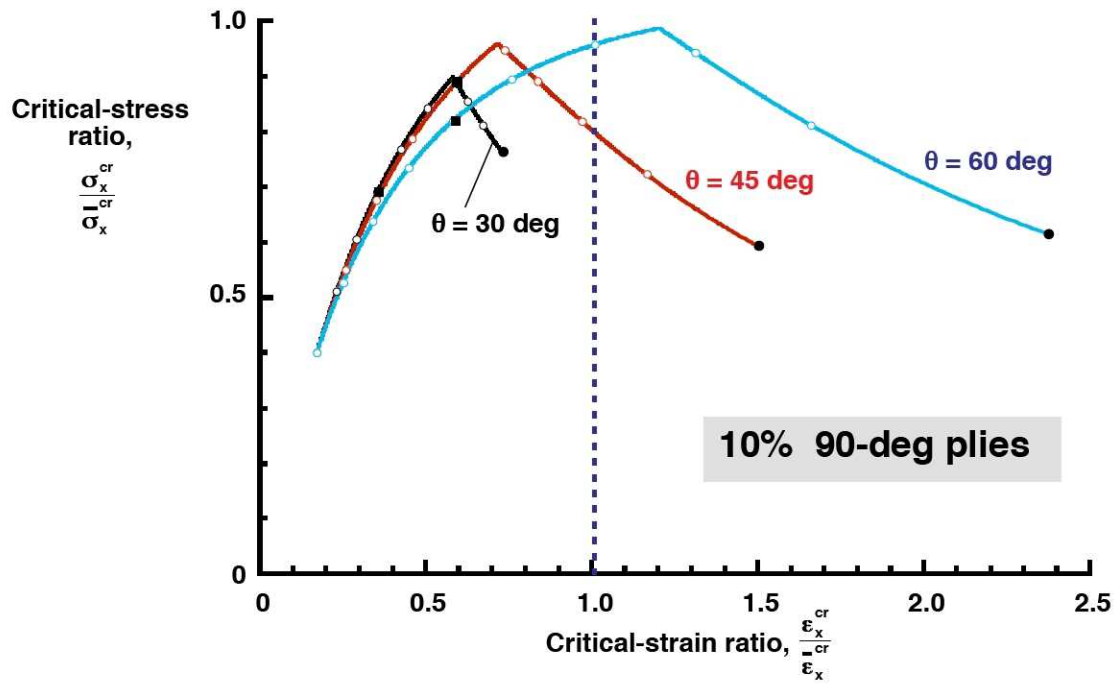
Figure 30. Effects of the fiber angle θ and the percentage of 0-degree plies on the critical-strain and critical-stress ratios for shell walls with 10% 90-degree plies.
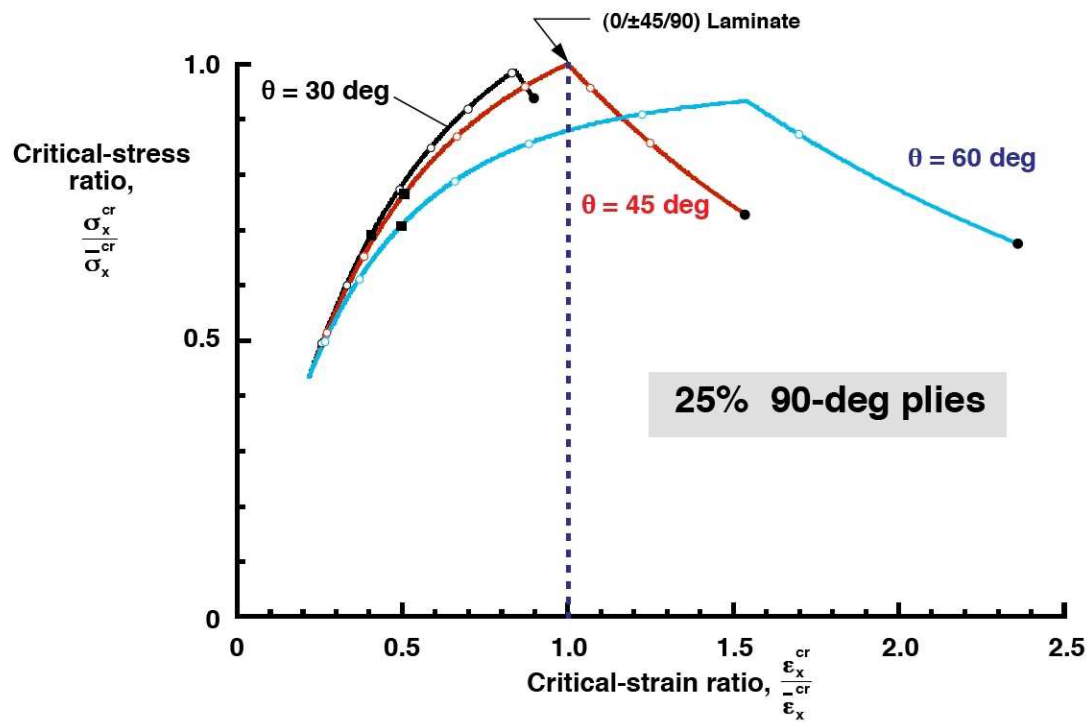
Figure 31. Effects of the fiber angle θ and the percentage of 0-degree plies on the critical-strain and critical-stress ratios for shell walls with 25% 90-degree plies.

47
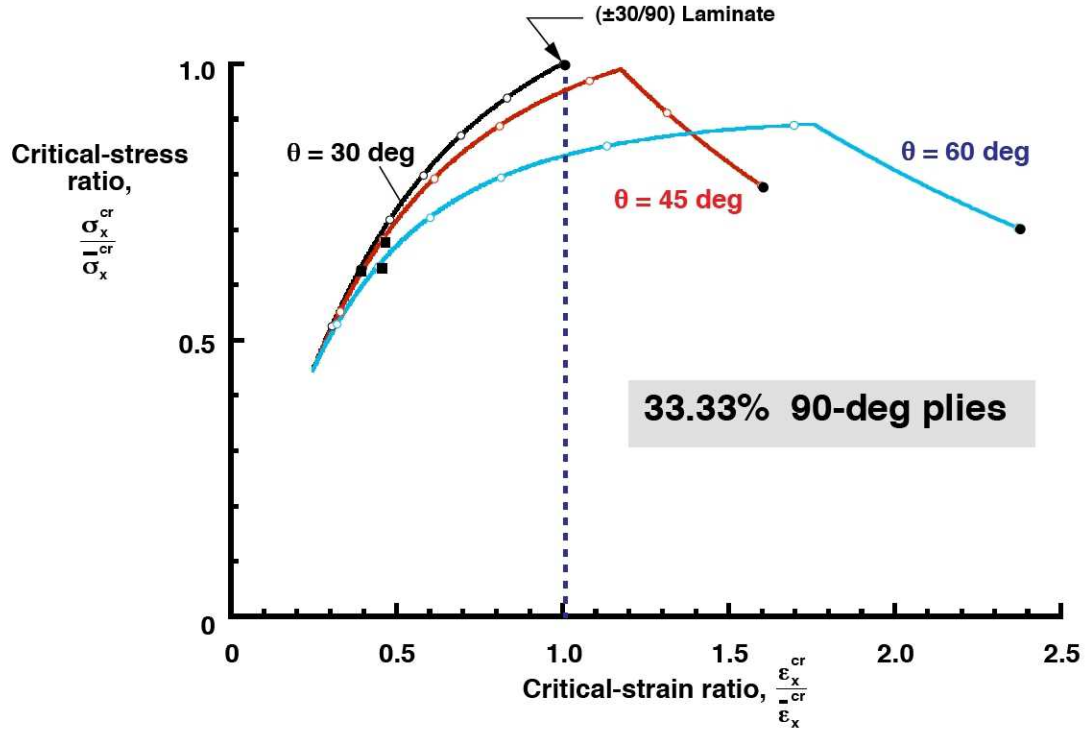
Figure 32. Effects of the fiber angle θ and the percentage of 0-degree plies on the critical-strain and critical-stress ratios for shell walls with 33.33% 90-degree plies.
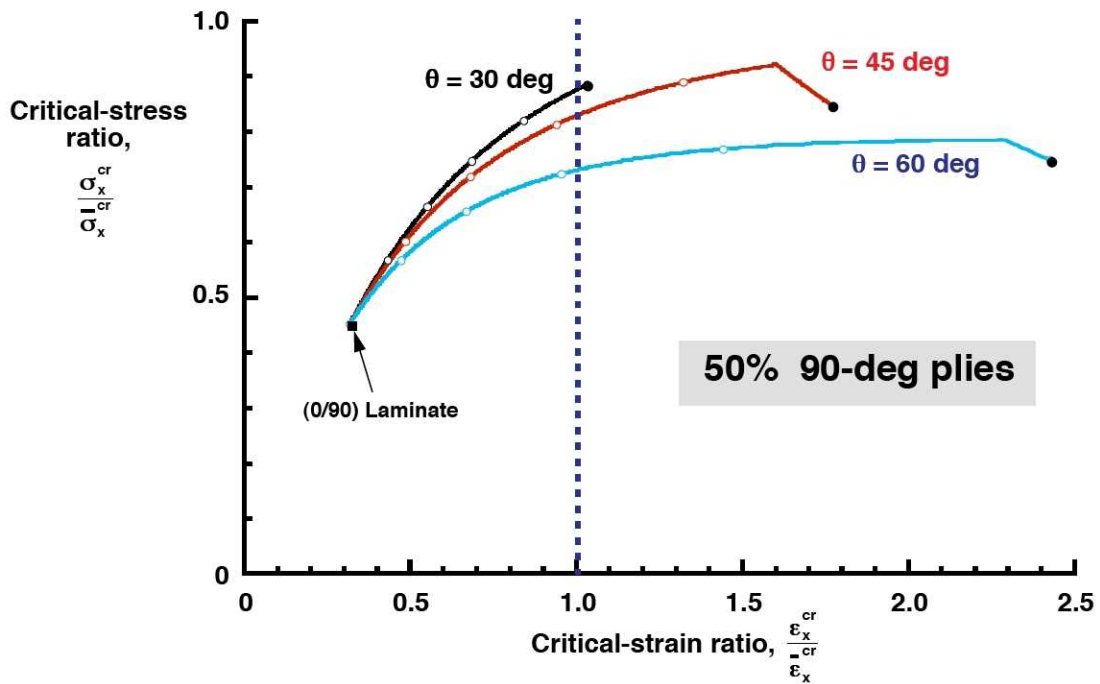
Figure 33. Effects of the fiber angle θ and the percentage of 0-degree plies on the critical-strain and critical-stress ratios for shell walls with 50% 90-degree plies.

48

Figure 34. Critical-strain and critical-stress ratios for selected laminates with no 90-degree plies.
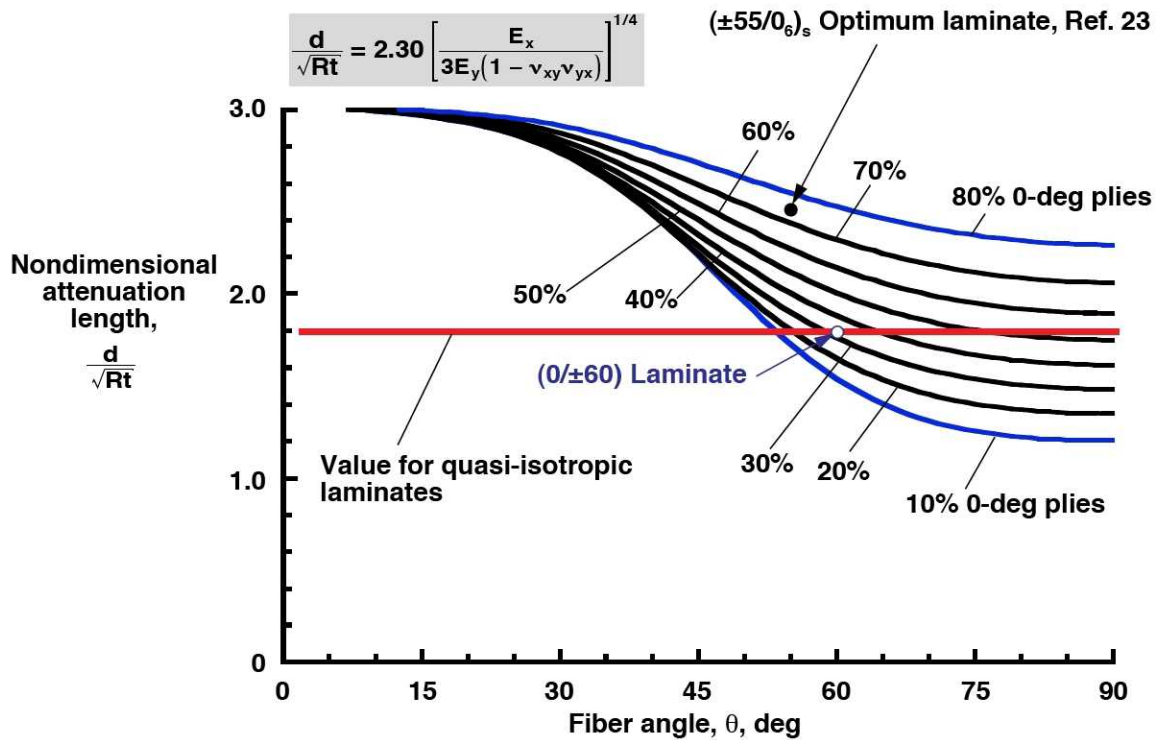
Figure 35. Effects of fiber angle and percentage of 0-degree plies on the nondimensional attenuation length for shell walls with no 90-degree plies.

$$\frac{d}{\sqrt{Rt}} = 2.30\left[\frac{E_x}{3E_y(1-\nu_{xy}\nu_{yx})}\right]^{1/4}$$
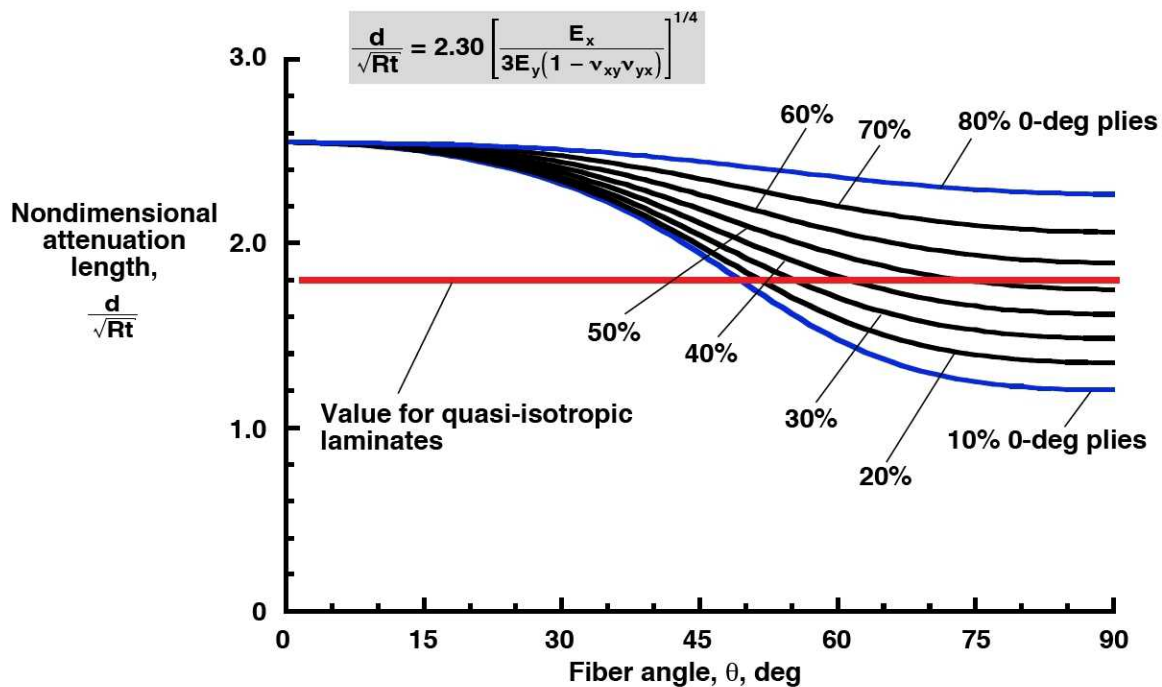
Figure 36. Effects of fiber angle and percentage of 0-degree plies on the nondimensional attenuation length for shell walls with 10% 90-degree plies.

$$\frac{d}{\sqrt{Rt}} = 2.30\left[\frac{E_x}{3E_y(1-\nu_{xy}\nu_{yx})}\right]^{1/4}$$
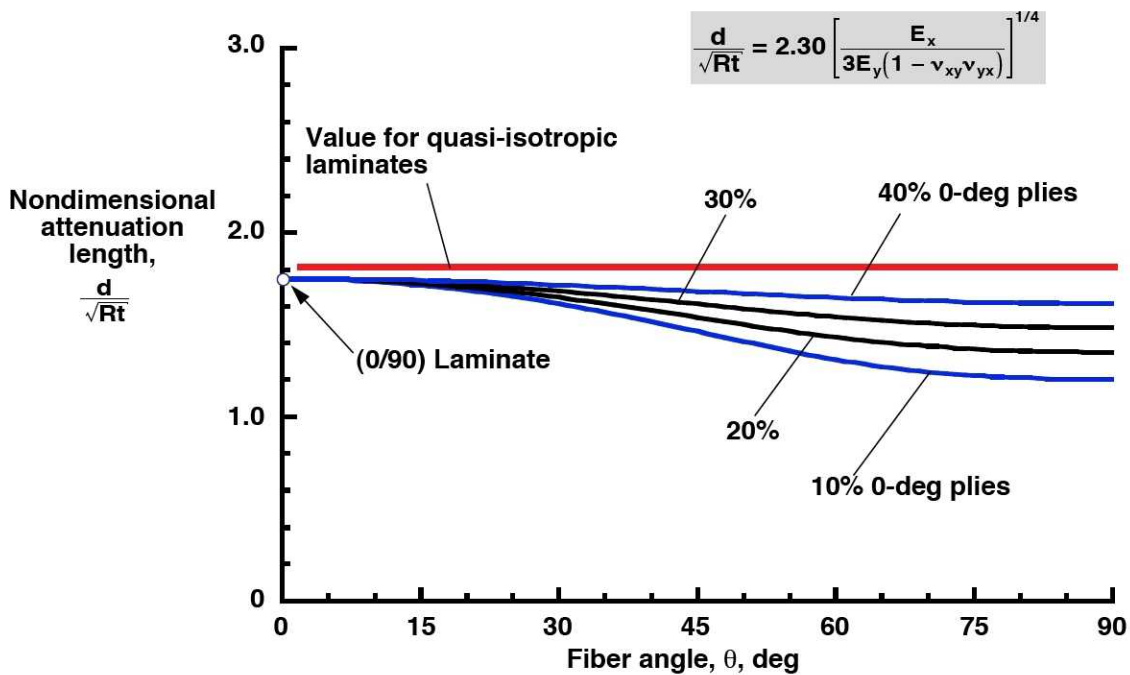
Figure 37. Effects of fiber angle and percentage of 0-degree plies on the nondimensional attenuation length for shell walls with 50% 90-degree plies.

1. REPORT DATE (DD-MM-YYYY) 01-08-2009	2. REPORT TYPE Technical Publication	3. DATES COVERED (From - To)

4. TITLE AND SUBTITLE Simple Formulas and Results for Buckling-Resistance and Stiffness Design of Compression-Loaded Laminated-Composite Cylinders	5a. CONTRACT NUMBER
	5b. GRANT NUMBER
	5c. PROGRAM ELEMENT NUMBER
6. AUTHOR(S) Nemeth, Michael P.; and Mikulas, Martin M., Jr.	5d. PROJECT NUMBER
	5e. TASK NUMBER
	5f. WORK UNIT NUMBER 136905.02.04.04.16.06

7. PERFORMING ORGANIZATION NAME(S) AND ADDRESS(ES) NASA Langley Research Center Hampton, VA 23681-2199	8. PERFORMING ORGANIZATION REPORT NUMBER L-19647

9. SPONSORING/MONITORING AGENCY NAME(S) AND ADDRESS(ES) National Aeronautics and Space Administration Washington, DC 20546-0001	10. SPONSORING/MONITOR'S ACRONYM(S) NASA
	11. SPONSORING/MONITORING REPORT NUMBER NASA/TP-2009-215778

12. DISTRIBUTION/AVAILABILITY STATEMENT

Unclassified-Unlimited
Subject Category 39   Availability: NASA CASI (443) 757-5802

13. SUPPLEMENTARY NOTES

An electronic version can be found at http://ntrs.nasa.gov

14. ABSTRACT

Simple formulas for the buckling stress of homogeneous, specially orthotropic, laminated-composite cylinders are presented. The formulas are obtained by using nondimensional parameters and equations that facilitate general validation, and are validated against the exact solution for a wide range of cylinder geometries and laminate constructions. Results are presented that establish the ranges of the nondimensional parameters and coefficients used. General results, given in terms of the nondimensional parameters, are presented that encompass a wide range of geometries and laminate constructions. These general results also illustrate a wide spectrum of behavioral trends. Design-oriented results are also presented that provide a simple, clear indication of laminate composition on critical stress, critical strain, and axial stiffness. An example is provided to demonstrate the application of these results to thin-walled column designs.

15. SUBJECT TERMS

Buckling; Shell mechanics; Structural design; Stability analysis; Composite cylinders

16. SECURITY CLASSIFICATION OF:			17. LIMITATION OF ABSTRACT	18. NUMBER OF PAGES	19a. NAME OF RESPONSIBLE PERSON STI Help Desk (email: help@sti.nasa.gov)
a. REPORT	b. ABSTRACT	c. THIS PAGE	UU	55	19b. TELEPHONE NUMBER (Include area code) (443) 757-5802
U	U	U			